nature materials

Supplementary information

https://doi.org/10.1038/s41563-024-01966-1

Helical peptide structure improves conductivity and stability of solid electrolytes

In the format provided by the authors and unedited

Table of Contents

1. Materials and instrumentation

1.1. Materials

All reagents and solvents were purchased from Sigma-Aldrich, TCI or Chem-Impex (e.g., amino acids) and used as received unless otherwise noted. Deuterated solvents were purchased from Cambridge Isotope Laboratories, Inc. (Tewksbury, MA, USA). Anhydrous tetrahydrofuran (THF), hexane, Ethyl acetate (EA), dichloromethane (DCM), *N*,*N*-dimethylformamide (DMF) were dried by a column packed with alumina. Silica gel (particle size 40-63 μm) was purchased from SiliCycle Inc. (Quebec City, Quebec, Canada) and desiccated by heating to 180 °C under vacuum for at least 48 h to remove water. γ-(3-chloropropanyl)-x-glutamate (ClP**X**G) and γ-(3-chloropropanyl)-x-glutamate *N*-carboxyanhydride (ClP**X**G-NCA), poly(γ-3-chloropropanyl-x-glutamate) (PClP**X**G), and poly(γ-3-azidopropanyl-x-glutamate) (PAP**X**G) were synthesized and purified according to literature procedures[1-3]. Alkyne-TFSI mimics was synthesized according to literature procedures[4,5]. Dialysis bags with 1 kDa, 5 kDa and 8 kDa molecular weight cutoff (MWCO) were purchased from Spectrum Labs.

1.2. Instrumentation

1.2.1. Nuclear magnetic resonance (NMR) Spectroscopy

^{1}H, ^{13}C and ^{19}F nuclear magnetic resonance (NMR) spectra were recorded on a Varian U500, VXR500, UI500NB, UI400 or a Bruker Carver B500 spectrometer in the NMR laboratory, University of Illinois. Chemical shifts reported in parts per million downfield from tetramethylsilane and referenced to the residual solvent peak. Carbon-13 Nuclear Magnetic Resonance (CP/MAS ^{13}C-NMR) spectra were obtained using a Varian UI300WB (300 MHz). MestReNova (version 12.0.3, Mestrelab Research, Escondido, CA, USA), provided by the NMR laboratory at University of Illinois, was used in the analysis of all NMR data.

1.2.2. Fourier-transform infrared spectroscopy (FTIR) and attenuated total reflectance (ATR-FTIR)

Fourier transform infrared (FTIR) spectra were performed using a Perkin Elmer 100 serial FTIR spectrophotometer (PerkinElmer, Santa Clara, CA, USA) calibrated with calibrated with polystyrene film. Specifically, a 100 μL solution (**X**-**DP**s in methanol, neutral polymers in DCM) was transferred to KBr plate and dried in air to form a solid film, that was then analyzed by FTIR. ATR-FTIR spectra was collected using a Bruker ALPHA FTIR spectrometer with a platinum-ATR QuickSnap sampling module and OPUS software. All samples were oven dried at least 2d at 120 °C before the measurements.

1.2.3. Size-exclusion chromatography (SEC)

Size-exclusion chromatography (SEC) was carried out on an instrument equipped with an isocratic pump (1260 Infinity II, Agilent, Santa Clara, CA, USA), a multi-angle static light scattering (MALS) detector with the detection wavelength at 658 nm (DAWN HELEOS-II, Wyatt Technology, Santa Barbara, CA, USA), and a differential refractometer (DRI) detector (Optilab T-rEX, Wyatt Technology, Santa Barbara, CA, USA). Separations were performed using serially connected size exclusion columns (three PLgel MIXED-B columns, 10 μm, 7.5 × 300 mm, Agilent, Santa Clara, CA, USA) at a temperature of 40 °C using DMF containing 0.1 M LiBr as the mobile phase at a flow rate of 0.7 mL/min. The MALS detector was calibrated using pure toluene and can be used for the determination of the absolute molecular weights (MWs). All polymer solutions (5mg/mL in DMF with 0.1 M LiBr) were filtered using a 0.45 μm PTFE filter before measurement. The MWs of polymers were determined based on the dn/dc value of each sample calculated offline by using the internal calibration system processed by the ASTRA 7 software (version 7.1.3.15, Wyatt Technology, Santa Barbara, CA, USA).

1.2.4. Circular dichroism (CD)

Circular dichroism (CD) measurements were carried out on a JASCO J-815 CD spectrometer (JASCO, Easton, MD, USA). For the solution phase, polymers were diluted to predetermined concentrations (0.5 mg/mL) in methanol and added into a quartz cell to measure with a wavelength range 180-300 nm. For the solid films, pre-dried polymers were hot-pressed to form transparent films with thickness about 100 μm by using Kapton with a hole as the spacer at 80 °C for 5 min. These films were then taped to quartz cells to test. The mean residue molar ellipticity of polypeptide in solution phase was calculated based on the measured apparent ellipticity by following the literature-reported formulas: Ellipticity ([θ] in deg cm^2 $dmol^{-1}$) = (millidegrees × mean residue weight) / (path length in millimeters × concentration of polypeptide in mg mL^{-1}).

1.2.5. Thermal gravimetric analysis (TGA)

Thermal gravimetric analysis (TGA, Q50-1110) was performed using a Q50 TGA with a TA Instrument Explorer software. All tests were used a platinum pan under ultrahigh purity nitrogen atmosphere and with a heating rate of 20 °C/min in the range of ambient temperature to 600 °C. All samples were fully dried before the measurements.

1.2.6. Differential scanning calorimetry (DSC)

Differential scanning calorimetry (DSC) measurements were taken out using a Discovery 2500 DSC (Q2500, TA instrument) with TRIOS software. All glass transition temperatures were collected under nitrogen atmosphere in hermetic pans with heating/cooling rate of 10 °C/min. The half point of change in heat capacity (1/2 ΔC_p method) in the second heating curve was used to determine the glass transition temperature of each polymer.

1.2.7 X-ray Scattering

Small-Angle X-ray Scattering (SAXS), Wide-Angle X-ray Scattering (WAXS), Grazing Incidence Small-Angle X-ray Scattering (GISAXS) and Grazing Incidence Wide-Angle X-ray Scattering (GIWAXS) data was collected using Xenocs GeniX3D Cu Kα X-ray source (beam size at sample 0.8 x 0.8 mm^2, wavelength 0.15418 nm) and a three-module Pilatus 300 detector with optional environmental controls. All sample preparations were conducted in glovebox: powder samples were sealed into capillary tubes made of quartz (1.5 mm, Hilgenberg); PPIL self-standing films were hot-pressed at 80 °C with 5 kg weight for 30 min; PPIL thin films were hot-pressed onto polished silicon wafers with same protocol. The sample-to-detector distance was calibrated with silver behenate powder and was ~1.4m for SAXS/GISAXS and ~0.14m for WAXS/GIWAXS. The scattering patterns were collected after 1h exposure time, and the 2D diffraction data were processed using FIT2D software.

1.2.8 Electrochemical Impedance Spectroscopy (EIS)

Electrochemical impedance spectra were recorded on SP-300 Potentiostat (Bio-Logic SAS, France) with an intermediate temperature system (ITS, Bio-Logic SAS, France). All preparations were conducted in a glovebox. Pre-dried polymer was placed in a hole (diameter 5 mm) of a Kapton spacer between two stainless-steel electrodes (with a thickness 0.5 mm), heated to 80 °C, and then pressed into a film and held for 2h. The hot-pressed polymer film thickness was determined by the average of three measurements with a micrometer. The cell was hermetically sealed by a crimper in the glovebox using a typical coin cell assembly (from top to bottom: anode cap, spring, stainless-steel electrode, polymer, Kapton, stainless-steel electrode, spring, cathode cap). The coin cell was first heated to 140 °C and equilibrium at least 4 h. The ionic conductivity over time was collected from high temperature to low temperature with a 5 °C or 10 °C temperature interval and a 60-min equilibration time was applied before each measurement. The applied voltage was 100 mV, and the frequency range was 10^6 Hz to 0.1 Hz. The impedance data was processed to make a plot of real (σ') and imaginary (σ") conductivities versus frequency, and the ionic conductivity of polymer electrolyte was taken as the real conductivity at the tan(δ) = σ'/ σ" maximum. Each polymer electrolyte was measured with three independent samples. The secondary structure of PPILs was checked after the measurement via ATR-FTIR to ensure the consistency of structure before and after measurement. Transference number cell (Li/Li symmetric cell) was prepared by placing hot-pressed film between two polished Li chips (with a diameter 16 mm and thickness 6 mm) with two layers of Kapton tape (with a diameter 5mm) as the spacer at 80 °C and then sealed with an assembly from top to bottom: anode cap, spring, stainless-steel electrode, Li chip, Kapton, polymer, Kapton, Li chop, stainless-steel electrode, spring, cathode cap. The cell was heated to 100 °C and equilibrium at least 4 h. An impedance spectrum (same setting with above) was first tested to ensure ionic conductivity consistency in two kinds of cells, and then Li transference number measurements were performed following a procedure in the literature[6]. The cell was charged (1h) and discharged (1h) with a current of 0.02 mA/cm^2 and repeated 6 times to stabilize the interface between the polymer and lithium. After 2h rest, impedance spectra

(1 MHz to1 Hz) were obtained with ΔV = 20 mV. Next, ΔV = 40 mV was applied and current was recorded for 2h to generate a steady current I_{ss}, followed by an impedance spectrum with an amplitude of 20 mV. The steady-state Li transference number was calculated via: $t_{ss}^{+} = \frac{I_{ss}}{I_{\Omega}}(\frac{\Delta V - I_{\Omega}R_0}{\Delta V - I_{ss}R_{ss}})$; where I_{Ω} ($I_{\Omega} = \frac{\Delta V}{R_T}$, R_T is the total cell resistance) is the initial current, I_{ss} is the steady state current, R_0 is the initial interfacial resistance, R_{ss} is the interfacial resistance when I_{ss} is reached. All R were obtained by fitting impedance spectra to an equivalent circuit R + L + R1/Q1 + R2/Q2. Three replicate cells were produced and tested.

1.2.9 Liquid chromatography–mass spectrometry (LC/MS)

LC/MS results were obtained using a 2.1 mm ID reverse phase C-18 column and Waters Q-TOF Ultima ESI in the Mass Spectrometry Laboratory at University of Illinois. The standard mobile phases are (A) 0.1% formic acid/water and (B) acetonitrile. The gradient setup of mobile phases over time: (1) 0 min: 95% A + 5% B; (2) 4 min: 50% A + 50% B; (3) 6 min: 50% A + 50% B; (4) 8 min: 5% A + 95% B.

1.2.10 Dielectric spectroscopy

Dielectric spectra were performed on Novocontrol C47 analyzer, which features the Novocontrol Alpha-A frequency response analyzer combined with PHECOS Lite temperature control system. Coin cells were sandwiched between two circulars, gold plated electrodes for testing. Temperature was controlled and stabilization was achieved by waiting for 300 s until the temperature change was less than 0.1 °C/min (max temperature error 0.1 °C). The cell contribution was subtracted form the measured impedance following literature protocol[7].

1.2.11 Elemental analysis

The iodide and fluorine contents of the PPILs were examined by Schöniger oxidation method and ion selective electrodes in the Microanalysis Laboratory at School of Chemical Sciences, University of Illinois, Urbana-Champaign.

1.2.12 Polarized optical microscopy (POM)

Micrographs were collected using a Zeiss Axioscope A1 microscope with 5x/10x/20x objective lens. Thin films were prepared by same protocol as the samples used for conductivity and X-ray measurements (80 °C with 5 kg weight for 30 min).

2. Experimental Procedures

2.1 synthesis of X-50s with different secondary structure

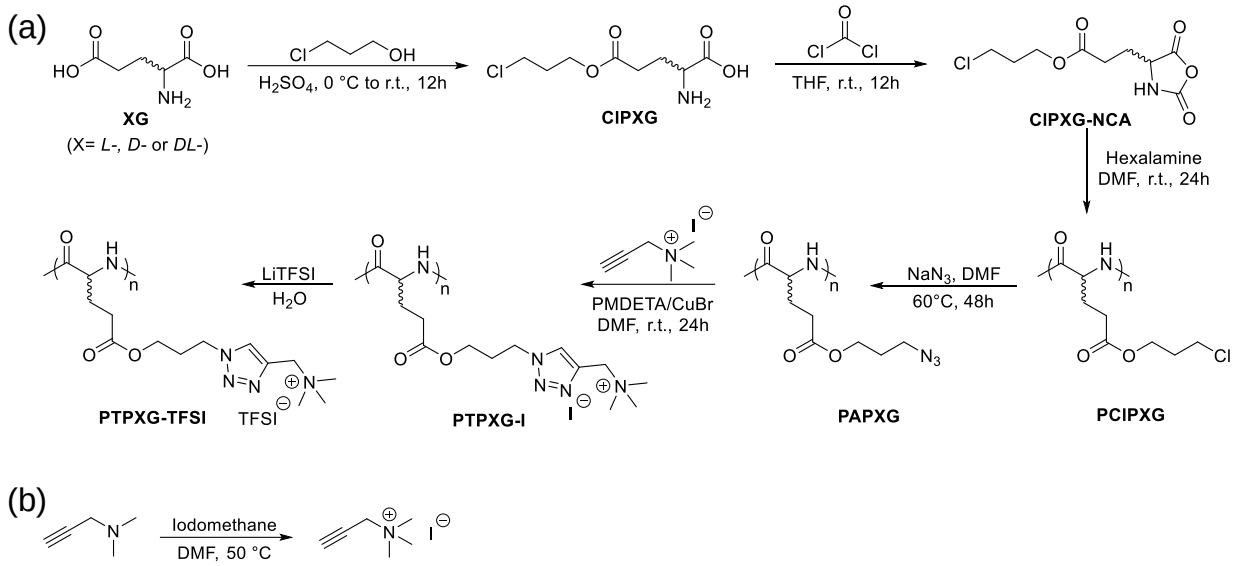

Supplementary Scheme 1. Synthesis route of (a) **X**-50s and (b) N,N,N-trimethyl-2-propynylammonium iodide.

ClP**X**G, ClP**X**G-NCA, PClP**X**G and PAP**X**G were synthesized according to literature procedures[1-3]. Briefly: (1) **X**G and 3-chloro-1-propanol were mixed and stirred over an ice bath, then sulfuric acid was slowly added. After stirring at room temperature for 1d, the reaction was neutralized by sodium bicarbonate solution to get the white solid that was then purified by recrystallization. (2) ClP**X**G was added into a flask and dried under vacuum with stirring for 2 h and dry THF was added forming a suspension. Phosgene solution (15 wt% in toluene) was added, and then the reaction was stirred overnight. The solvent was removed under vacuum, and crude product was purified by chromatography to yield a light yellow solid CIP**X**G-NCA. (3) PCIP**X**G was synthesized by ring opening polymerization (ROP) of CIP**L**G-NCA at room temperature in DMF with hexylamine as the initiator ($[M]_0/[I]_0 = 50$), followed by precipitation in cold hexane/ether (1:1, v/v) twice. (4) PCIP**X**G was dissolved in DMF first, and then sodium azide (NaN_3) was added. After stirring at 60 °C for 2d, the insoluble portion was removed by filtration, and the filtrate was concentrated and then precipitated in methanol to yield yellow solid PAP**X**G. The chemical structures of each step was confirmed by ^{1}H NMR and ^{13}C NMR.

Synthesis of Alkyne-functionalized ammonium salt (N,N,N-trimethyl-2-propynylammonium iodide). 3-dimethylamino-1-propyne (1 mL, 9.28 mmol) was dissolved in anhydrous DMF (2 mL) and the solution of iodomethane (578 µL, 9.28 mmol) was added. The mixture was stirred at 50 °C overnight, followed by precipitation in 40 mL ether solvent. The precipitate was washed by ether three times, and then N,N,N-trimethyl-2-propynylammonium iodide was obtained as an off-white solid (2.2 g, ~98%

yield). The structure was confirmed by ^{1}H NMR (500 MHz) and ^{13}C NMR (125 MHz) in TFA-d. ^{1}H NMR: δ (ppm) 4.53 (s, 2H), 3.58 (s, 9H), 3.17 (s, 1H). ^{13}C NMR: δ (ppm) 81.54, 68.90, 57.06, 52.92.

Synthesis of PTPXG-Is by copper-catalyzed click reaction in Glovebox. The reaction molar ratio of PAP**X**G/alkyne-functionalized ammonium salt/PMDETA/CuBr/Sodium-L-ascorbate was 1/1.5/1/1/1. For example, PAPLG (400 mg, 1.89 mmol), N,N,N-trimethyl-2-propynylammonium iodide (640 mg, 2.84 mmol), PMDETA (327 mg, 1.89 mmol), CuBr (270 mg, 1.89 mmol) and Sodium-L-ascorbate (374 mg, 1.89 mmol) were dissolved in anhydrous DMF (10 mL). The mixture was stirred at RT for 2d. The mixture was quenched by exposing to air for 1h and the color was changed from yellow to blue. Impurities and unreacted salt were removed by dialysis (MWCO=1 KDa) in saturated EDTA solution until the polymer solution in the dialysis bag changed from blue to colorless, and then continued to dialyze in DI water for 3d.

Ion exchange. LiTFSI salt (5.42 g, 18.9 mmol, 10 equiv.) was dissolved in DI water (5mL) and then mixed with the polymer (PTPLG-I) solution in the dialysis bag. The DI water was switched every two hours to remove the excess LiTFSI and LiI salt until the ionic conductivity of the dialysis solution is lower than 2 μS/cm. The final polymer (PTP**X**G-TFSI, also called **X**-50s) was precipitated in the dialysis bag. They were collected by centrifugation, lyophilized for 2d, vacuum dried at 400 K for another 2d, and then stored in glovebox for further use.

The obtained three PPILs (**L**-50, **D**-50 and **LD**-50) were confirmed by ^{1}H NMR, ^{13}C NMR and ^{19}F NMR.

2.2 Synthesis of negatively charged polypeptide PILs

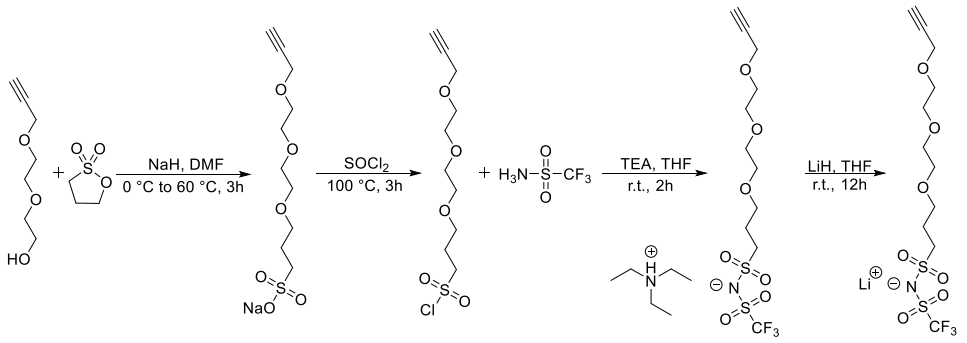

Supplementary Scheme 2. Synthesis of alkyne-TFSI.

Synthesis of Alkyne-functionalized TFSI-mimics salt. Alkyne-TFSI was synthesized according to literature procedures[4,5].

Step 1: NaH (60% in mineral oil, 1.21 g, 30 mmol) was dissolved in anhydrous DMF (25 mL) on an ice bath and the solution of 2-(2-(2-Propynyloxy)ethoxy)ethanol (4.36 g, 30 mmol) in DMF (25 mL) was added dropwise over 10 min. A solution of 1,3-propanesultone (3.66g, 30 mmol) in DMF (25 mL) was then added dropwise for 10 min. The mixture was stirred on an ice batch for 10 min and then heated to 60 °C for 3h. The DMF was removed by rotary evaporation and the residue was washed by diethyl ether to yield a white solid, compound 1. ^{1}H NMR (500 MHz, CD_3OD): δ (ppm) 4.11 (d, *J* = 2.5 Hz, 2H), 3.35-3.58 (m, 10H), 2.55 (t, *J* = 2.5 Hz, 1H) 2.40-2.49 (m, 2H), 1.78 (m, 2H); ^{13}C NMR (125 MHz): δ (ppm) 78.7, 76.4, 70.9, 70.6, 70.4, 70.2, 69.5, 60.5, 48.6, 24.3.

Step 2: Compound 1 (6.58 g, 22.8 mmol) and thionyl chloride (12 mL, 168 mmol) was mixed and heated to 100 °C under N_2 for 3h. The mixture was concentrated to yield brown oil and then dissolved in benzene (20 mL). The solvent was removed by evaporator and dissolved in DCM (50 mL). The insoluble salt was removed by filtration and filtrate was concentrated to yield a yellow oil, compound 2. ^{1}H NMR (500 MHz, CD_3OD): δ 4.19 (d, *J* = 2.5 Hz, 2H), 3.88-3.78 (m, 2H), 3.57-3.72 (m, 10H), 2.41 (t, *J* = 2.5 Hz, 1H), 2.40-2.49 (m, 2H); ^{13}C NMR (125 MHz): δ 79.9, 75.4, 70.9, 70.8, 70.4, 70.2, 68.5, 63.0, 58.6, 24.3.

Step 3: Trifluoromethanesulfonamide (3 g, 20 mmol) and triethylamine (5.6 mL, 40 mmol) were dissolved in anhydrous THF (20 mL) and the solution of compound 2 (5.7 g, 20 mmol) in THF (10 mL) was added dropwise. The mixture was stirred at RT for 2h. The insoluble salt was removed by filtration and the filtrate was concentrated and dissolved in DCM, followed by washing with distilled water four times. The organic phase was dried with anhydrous $MgSO_4$ and then the solvent was removed by evaporation to yield a yellow liquid. ^{1}H NMR (500 MHz, $CDCl_3$): δ (ppm) 4.20 (d, *J* = 3 Hz, 2H), 3.53-3.73 (m, 10H), 3.24-3.29 (m, 2H), 2.44 (t, *J* = 2.5 Hz, 1H), 2.08-2.16(m, 2H); ^{13}C NMR (125 MHz): δ (ppm) 160.5, 78.7, 76.4, 70.7, 70.6, 70.4, 69.5, 69.2, 60.3, 55.3, 45.5, 20.2, 8.7; ^{19}F NMR: -77.9.

Step 4: Compound 3 (6 g, 12 mmol) was dissolved in anhydrous THF (10 mL) in glovebox and lithium hydride (0.2 g, 25 mmol) was added slowly to minimize bubble production. The mixture was stirred at RT overnight. The insoluble salt was removed by filtration and the filtrate was concentrated. The residue was washed with hexane (50 mL) twice and then dissolved in water (80 mL). The aqueous solution was washed with diethyl ether (40 mL) four times. The solvent was removed by lyophilized for 2d to yield the final product. ^{1}H NMR (500 MHz, D_2O): δ (ppm) 4.24 (d, *J* = 2.5 Hz, 2H), 3.74-3.77 (m, 2H), 3.66-3.73 (m, 8H), 3.31-3.36 (m, 3H), 2.06-2.14 (m, 2H); ^{13}C NMR (125 MHz): δ (ppm) 165.1, 78.7, 76.4, 75.2, 70.5, 70.4, 70.0, 69.5, 60.3, 40.1, 20.1; ^{19}F NMR: -78.6.

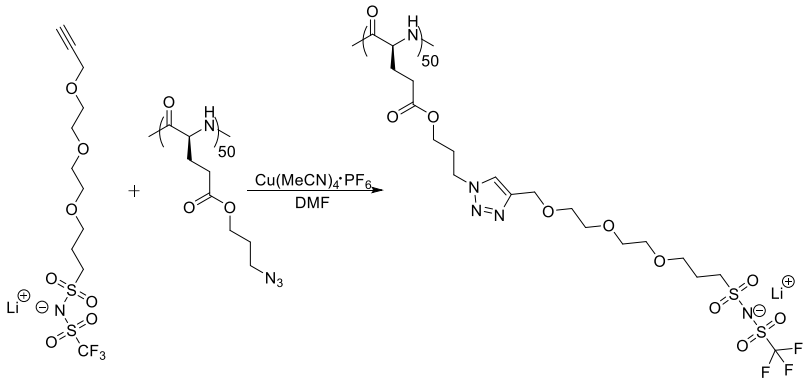

Supplementary Scheme 3. Synthesis of negatively charged polypeptide PIL, L50-3EO-TFSI/Li.

Synthesis of L50-3EO-TFSI/Li by copper-catalyzed click reaction. PAPLG (0.4 g, 1.9 mmol), compound 3 (1.16 g, 2.9 mmol) and tetrakis(acetonitrile)copper(I) hexafluorophosphate ($Cu(MeCN)_4 \cdot PF_6$, 110 mg, 0.3 mmol) was dissolved in anhydrous DMF (5 mL) in a Schlenk flask. The mixture was freeze-pump-thawed three times and then heated at 60 °C for 24h. After cooling down to RT, the solution was treated with the metal scavenger (QuadraPure TU, 1.0 g) for 30 min under air twice. After the filtration, the solution was transferred into 1 kDa MWCO dialysis bag and dialyzed in LiTFSI solution (10 g dissolved in 500 mL DI water) for 3d, and then continued to dialyze in DI water until the ionic conductivity of the dialysis solution is lower than 2 μS/cm. The solvent was removed by lyophilizer for 2d, vacuum drying at 400 K for another 2d, and the final product was stored in glovebox for further use.

The final negatively charged polypeptide PIL, L50-3EO-TFSI/Li, were confirmed by ^{1}H NMR, ^{13}C NMR and ^{19}F NMR in D_2O and DMF-*d*.

2.3 Synthesis of L-DPs

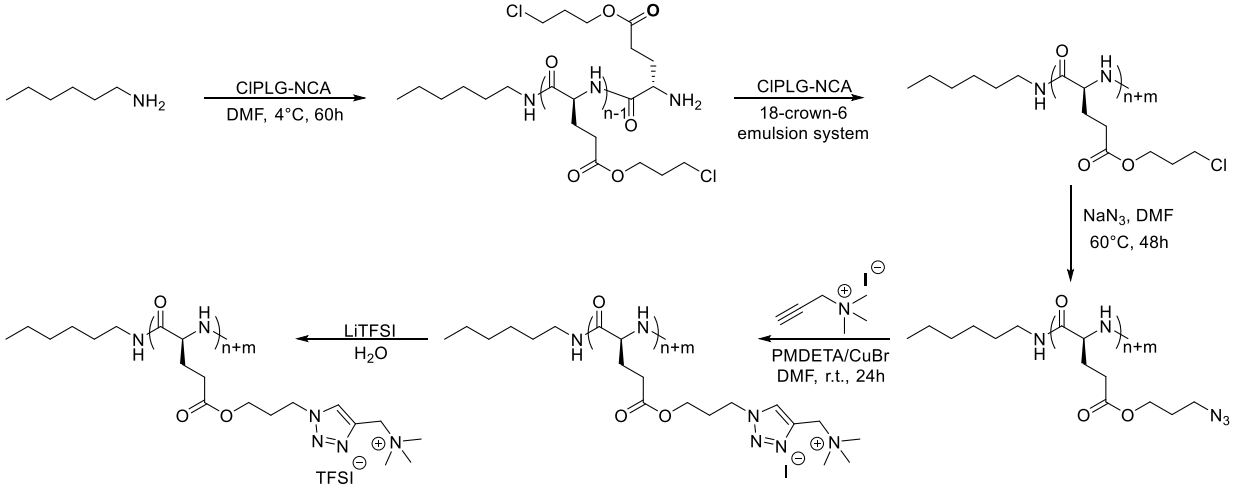

Supplementary Scheme 4. Synthesis of helical PPILs with different DP.

Synthesis of the PClPLG$_{50}$-NH$_2$ macroinitiator. 100 mM hexylamine DMF solution (400 μL, 0.04 mmol) was added to the 500 mM ClPLG-NCAs DMF solution (4 mL, 2 mmol) to initiate the ROP. The mixture was kept at 4 °C for 60h, and then precipitated in the cold hexane/ether (v/v=1/1). The obtained polymer was dissolved in DCM and precipitated again. The final product was collected by centrifugation and dried in vacuum at low temperature, and stored in -20 °C. The structure of PClPLG$_{50}$-NH$_2$ was confirmed by ^{1}H NMR, the DP (~50) was determined by GPC and NMR end group analysis.

Synthesis of PClPLG with different MW using PClPLG-NH$_2$ as macroinitiator. The polymerization of PClPLG with higher MW was achieved by using PClPLG$_{50}$-NH$_2$ macroinitiator-initiated ROP in emulsion system ($V_{DCM}/V_{pH=7\ buffer}$= 95 % / 5 %) with crown ether as catalyst[8,9]. For PClPLG$_{250}$ as an example, 1 mM PClPLG$_{50}$-NH$_2$ DCM solution (6 mL, 0.006 mmol, 1 eq), 200 mM ClPLG-NCAs DCM solution (6 mL, 1.2 mmol, 200 eq), crown ether (3.1 mg, 0.01 mmol, 2 eq) and pH=7 buffer (0.6 mL) were mixed together. The mixture was allowed to stir at RT for 24 h. The water was removed by using anhydrous Sodium sulfate, and the organic phase was concentrated to only 1-2 mL left before precipitating in hexane/ether (v/v=1/1) twice. The product was collected by centrifugation and dried in vacuum. The structure of PClPLG$_{50}$-NH$_2$ was confirmed by ^{1}H NMR, the MW was determined by GPC.

The ionic functionalization followed the procedure in section 2.1. The obtained polymers, **L**-DPs, were confirmed by ^{1}H NMR, ^{13}C NMR and ^{19}F NMR in TFA-*d*.

2.4 Degradation of PPILs

L-50 (right-handed helix), **D**-50 (left-handed helix), **LD**-50 (random coil) and **L**-498 (longer right-handed helix), were exposed to 6 M HCl with a concentration of 2 mg/mL at 110 °C, and completely degraded after 1 day. The reaction solvent was removed under vacuum and the obtained solid products were characterized by ^{1}H NMR in TFA-*d*. The solid mixtures were also dissolved in DI water with a concentration of 1 mg/mL, and then analyzed by HPLC and LC-MS.

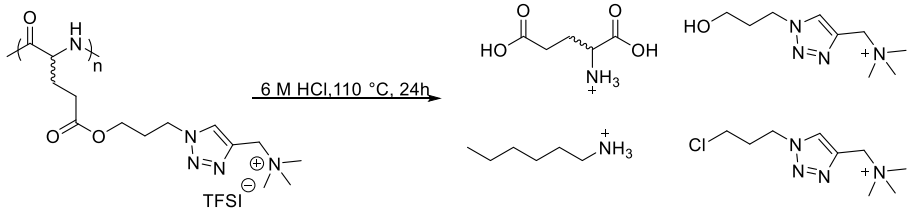

Supplementary Scheme 5. Degradation of PPILs.

2.5 Hot-pressed PPIL self-standing films and coin cell preparation

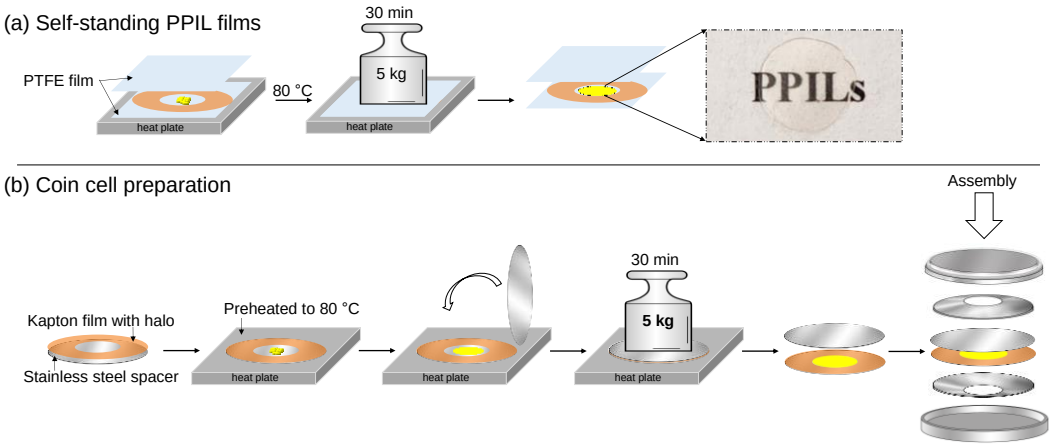

Supplementary Scheme 6. Schematic illustration of (a) hot-pressed PPIL self-standing films and (b) coin cell preparation in glovebox.

3. Supplementary Figures and Tables

3.1 Polypeptides with different secondary structures

(a)

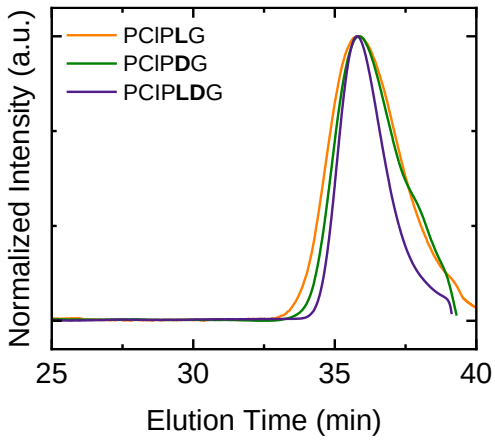

(b)

Polymer	M_n (kDa) *	M_w (kDa)*	$Đ$*	DP*	DP**
PCIP**L**G	10.01	11.41	1.11	49	50
PCIP**D**G	10.55	11.70	1.10	51	50
PCIPL**D**G	10.60	11.45	1.08	51	50

* determined by SEC ** determined by NMR

Supplementary Figure 1. (a) SEC-LS traces of three polypeptide backbone PCIP**X**Gs initiated by hexylamine in DMF of GIP**X**G-NCAs. $[M]_0$ = 50 mM, $[M]_0/[I]_0$ = 50. (b) Comparison table of their degree of polymerization (DP) determined by SEC (*) and NMR (**) end group analysis.

ClPXGs:

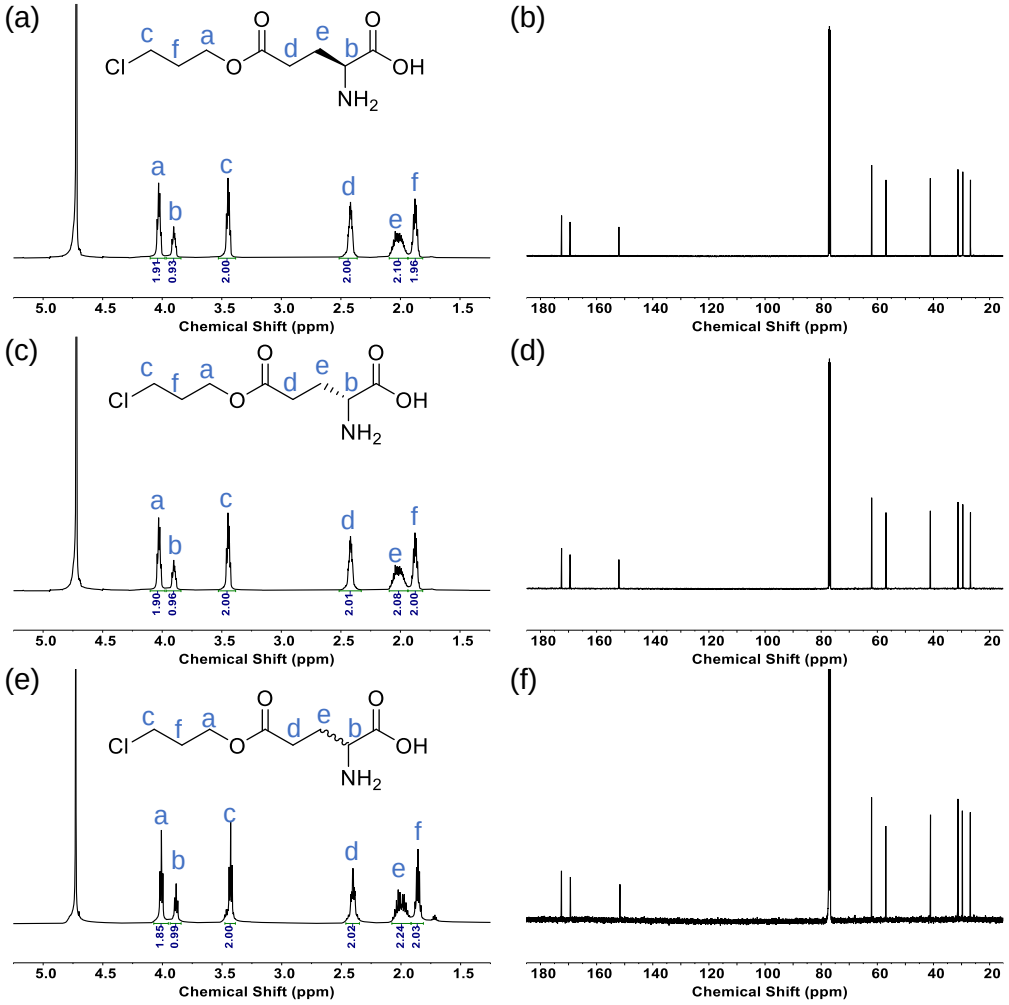

Supplementary Figure 2. ^{1}H-NMR and ^{13}C-NMR spectra of ClP**X**Gs in D_2O.

ClPXG-NCAs:

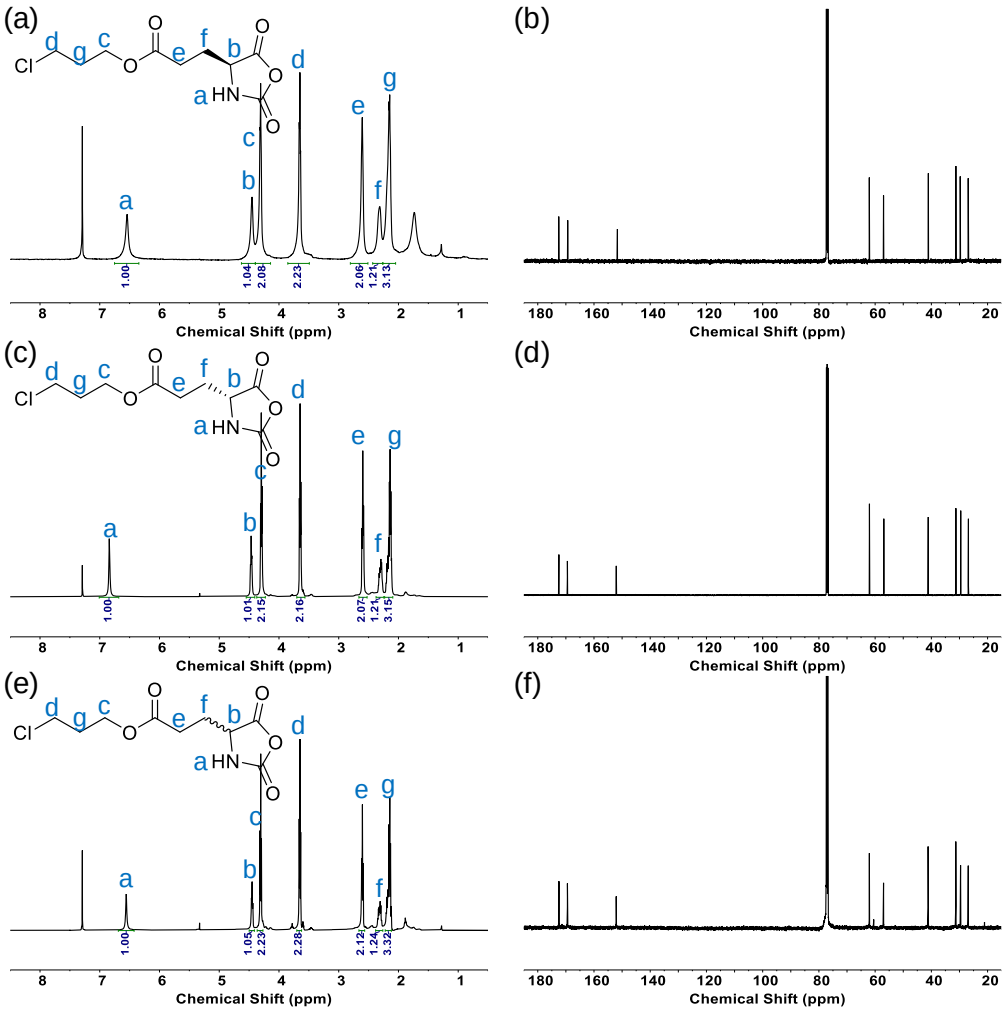

Supplementary Figure 3. ^{1}H-NMR and ^{13}C-NMR spectra of ClP**X**G-NCAs in $CDCl_3$.

PClPXGs:

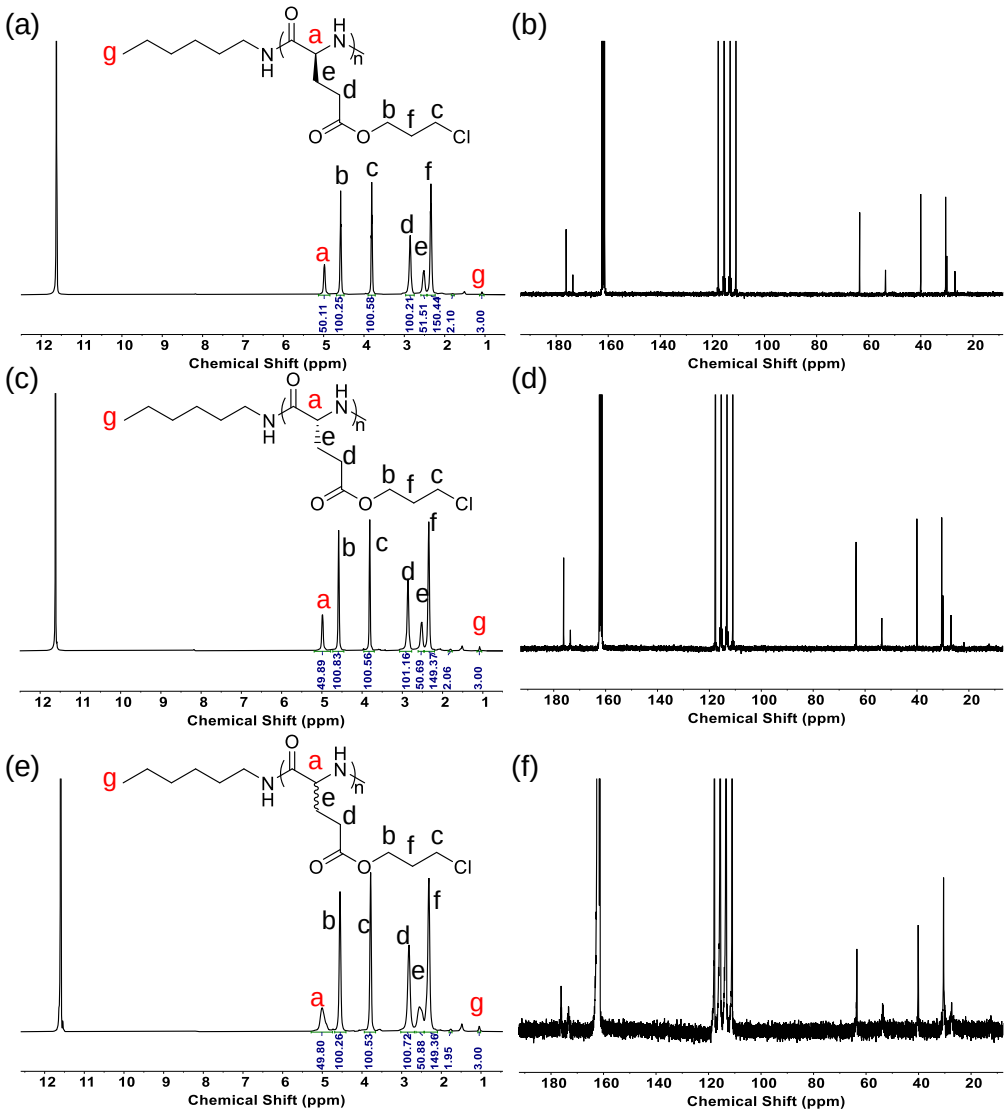

Supplementary Figure 4. ^{1}H-NMR and ^{13}C-NMR spectra of PClP**X**Gs in TFA-*d*. End group analysis: the integration of hydrogen in methyl group [peak g] was fixed at 3.00, and the integration of hydrogen in center carbon [peak a] equals to the absolute DP**. All these three polymers have a similar DP**=50.

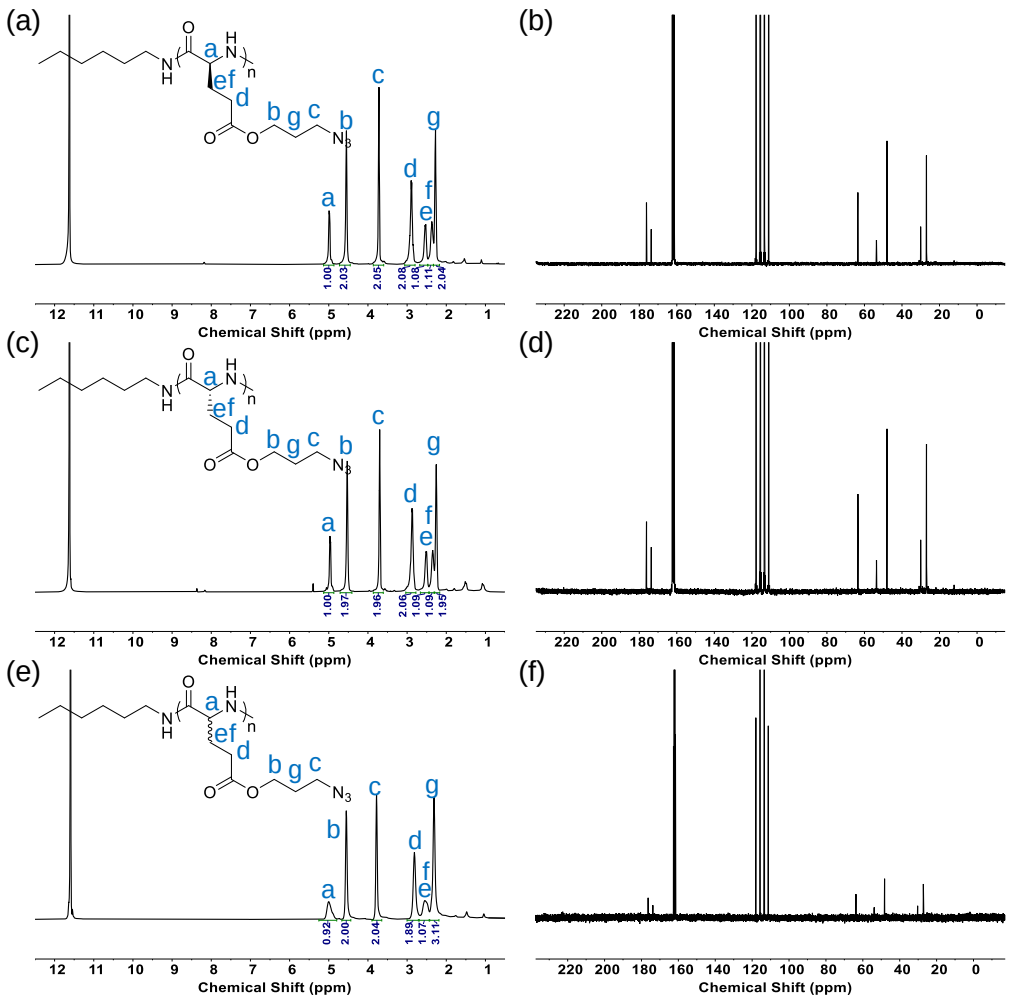

Supplementary Figure 5. ^{1}H-NMR and ^{13}C-NMR spectra of PAP**X**Gs in TFA-*d*.

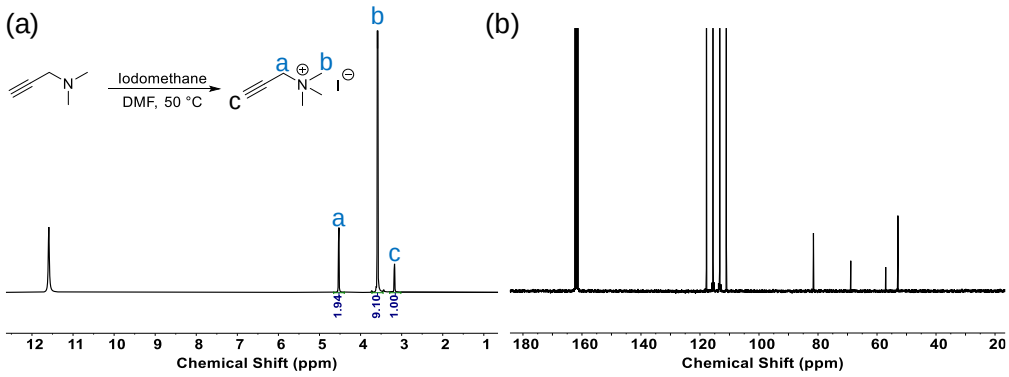

Supplementary Figure 6. ^{1}H-NMR and ^{13}C-NMR spectra of N,N,N-trimethyl-2-propynylammonium iodine in TFA-*d*.

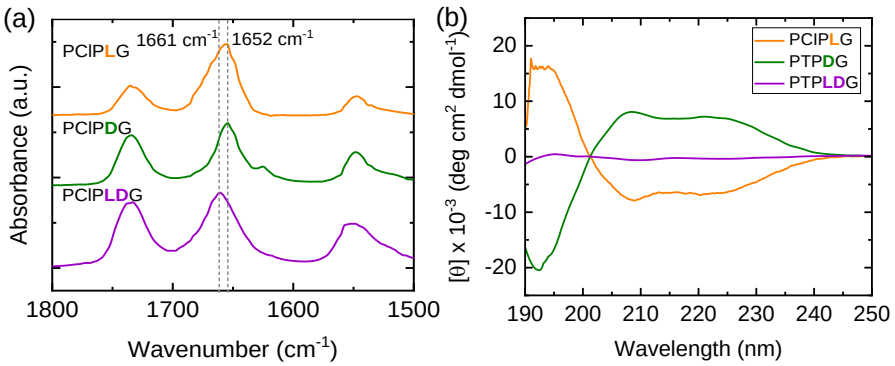

Supplementary Figure 7. (a) Stacked FTIR spectra and (b) CD spectra of PCIP**X**Gs. PCIP**L**G (orange) adopted a right-handed helical conformation, evidenced by the characteristic absorbance peaks of amide I at 1652 cm^{-1} in the FTIR spectra and characteristic double minima at 208 nm and 222nm in the CD spectra; PCIP**D**G (green) adopted a left-handed helical conformation based on the characteristic absorbance peaks of amide I at 1652 cm^{-1} and characteristic double maxima at 208 nm and 222nm; however, PCIP**LD**G adopted a random coil conformation, as evidenced by the characteristic absorbance peaks of amide I at 1661 cm^{-1} and negligible intensity in CD spectra.

PTPLG-TFSI (L-50):

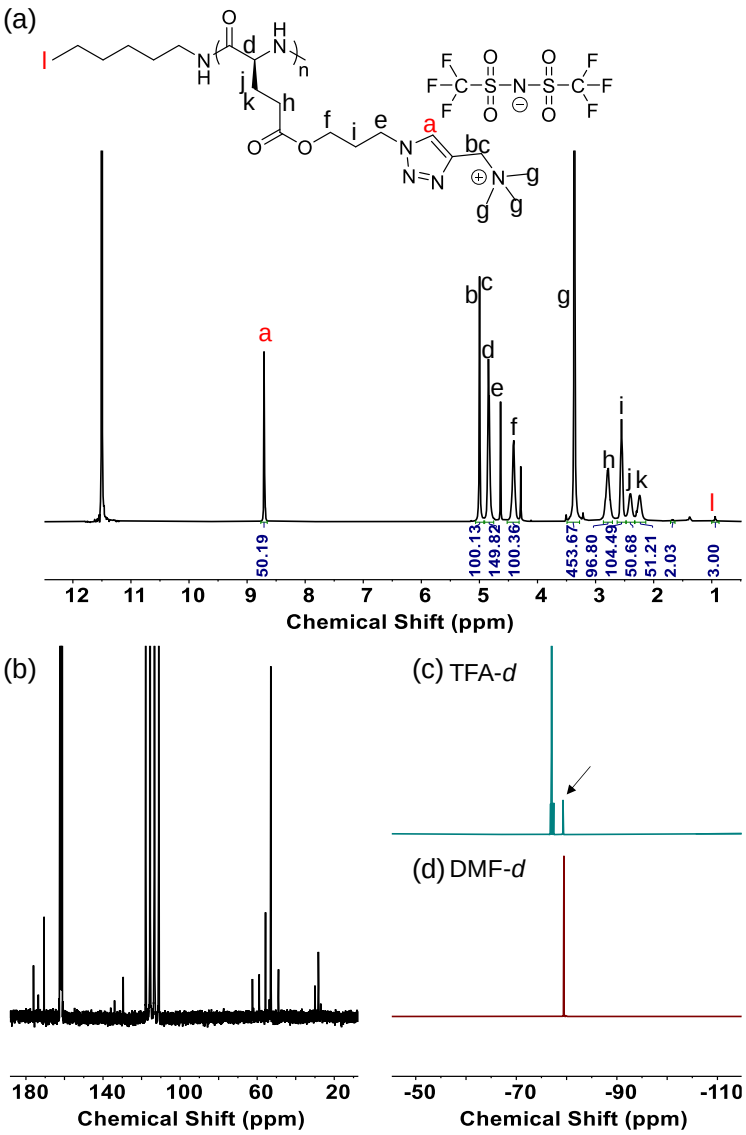

Supplementary Figure 8. (a)^{1}H-NMR, (b)^{13}C-NMR and (c)^{19}F-NMR spectra of **L**-50 in TFA-*d*. The integration ratio of [peak a] and [peak l] were used to determine the absolute DP** by end group analysis. The obtained DP value of **L**-50 was 50, which is consistent with the polymer precursor (PCIP**L**G), indicating the chemical stability of the backbone after post modifications. The quantitative conversion of side chain was also confirmed by the molar ratio of polypeptide (peak d or peak a) and quaternary ammonium salt (e.g., peak g) was 1:1. (d) ^{19}F-NMR spectra of **L**-50 in DMF-*d*. Given the strong signal of TFA-*d* and its proximity to the signal peak position of our PPILs, we used DMF-*d* as the solvent for further confirmation. In DMF-*d*, only a single peak is detected, originating solely from the sample under investigation.

PTPDG-TFSI (D-50):

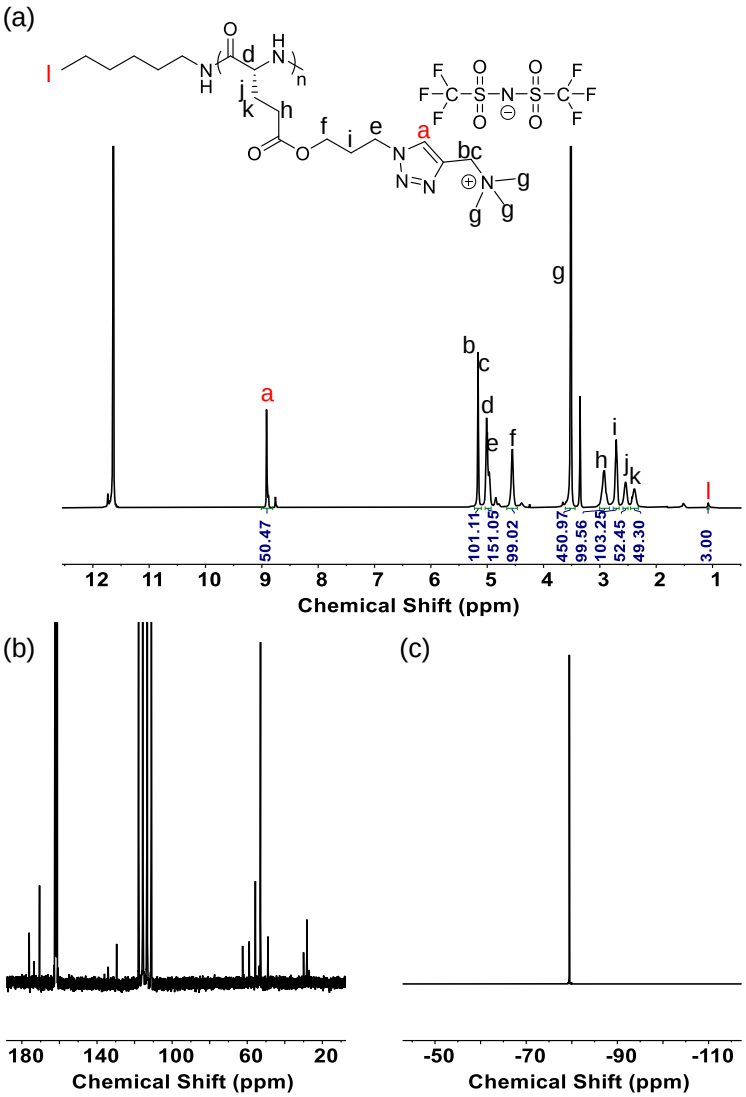

Supplementary Figure 9. (a)^{1}H-NMR and (b) ^{13}C-NMR spectra of **D**-50 in TFA-*d*. The final DP of **D**-50 was confirmed to be 50 by the integration ratio of [peak a] and [peak l], that was similar with its precursor PCIP**D**G. The quantitative conversion of side chain was also confirmed by the proton integration of [peak a] and [peak g]. (c) ^{19}F-NMR spectra **D**-50 in DMF-*d*.

PTPLDG-TFSI (LD-50):

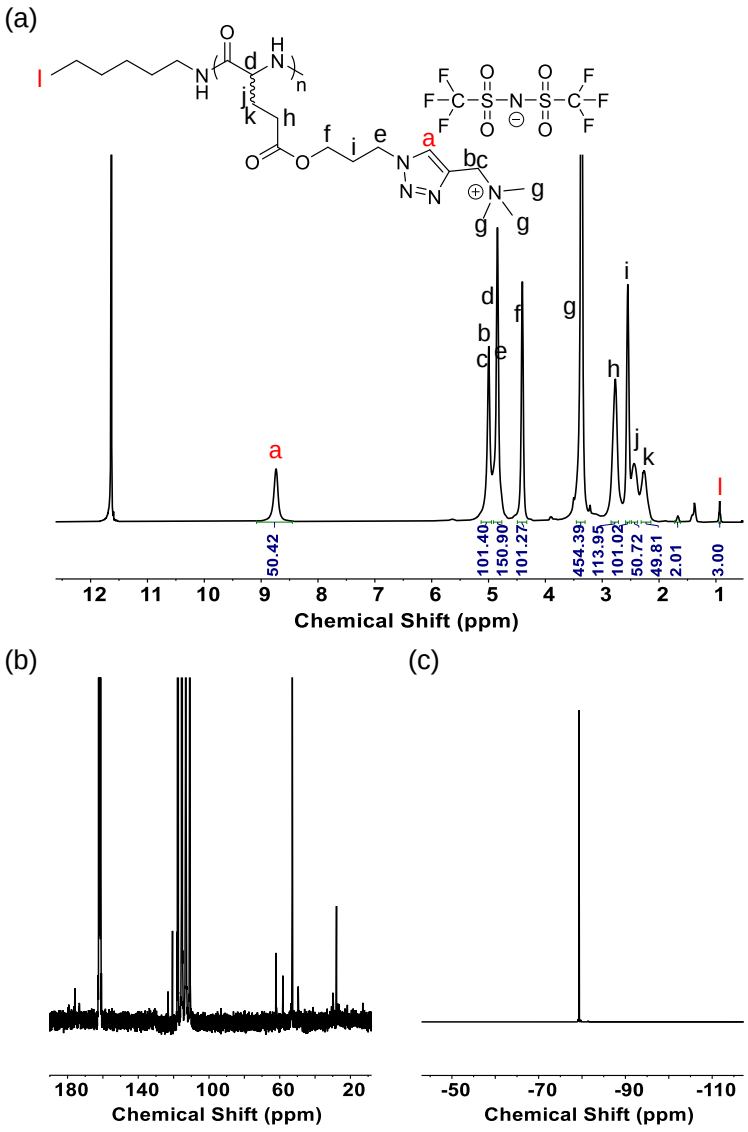

Supplementary Figure 10. (a)^{1}H-NMR and (b) ^{13}C-NMR spectra of **LD**-50 in TFA-*d*. The final DP of **LD**-50 was confirmed to be 50 by the integration ratio of [peak a] and [peak l], that was similar with its precursor PCIP**LD**G. The quantitative conversion of side chain was also confirmed by the integration of [peak a] and [peak g]. (c) ^{19}F-NMR spectra **LD**-50 in DMF-*d*.

Supplementary Table 1. Elemental analysis of PPILs

PPILs	I wt. %		F wt. %	
	actual	theoretical	actual	theoretical
L -50	0.06 %		19.90 %	
D -50	0.00 %		19.70 %	
LD -50	0.16 %		19.35 %	
L-233	0.01 %	0.0%	18.64 %	19.3 %
L-498	0.01 %		18.60 %	
L-768	0.01 %		19.23 %	
L-925	0.01 %		19.67 %	

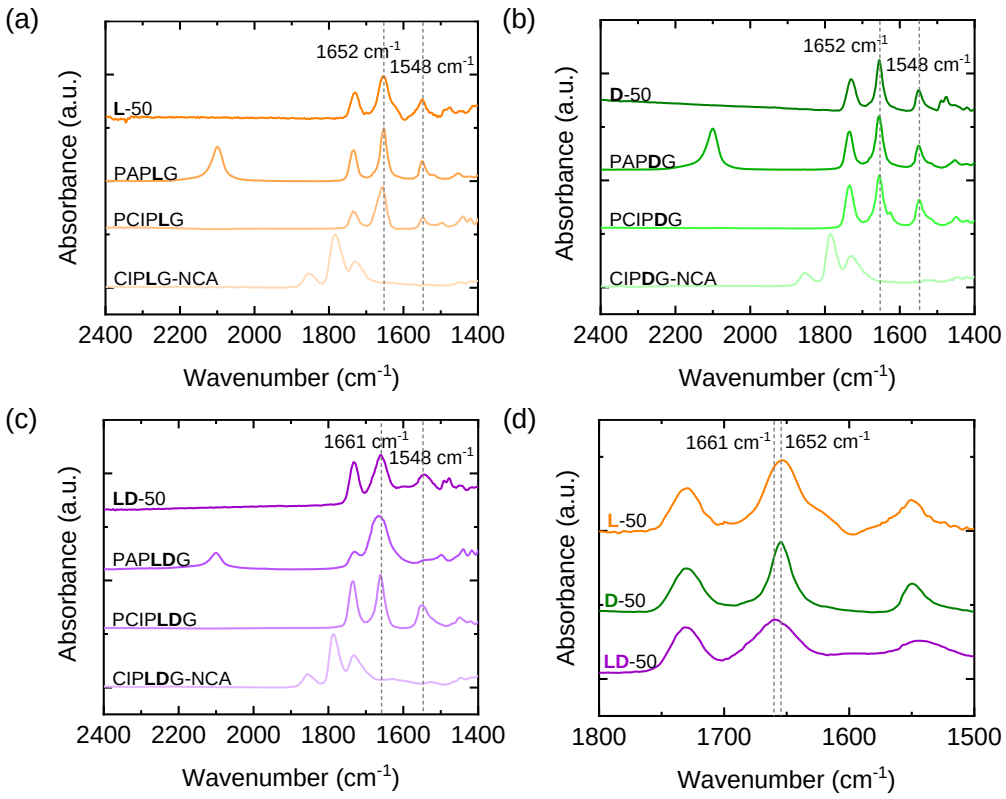

Supplementary Figure 11. Stacked FTIR spectra of synthetic products (CIP**X**G-NCAs, PCIP**X**Gs, PAP**X**Gs, **X**-50s) in each step. After polymerization of CIP**X**G-NCAs, the intensity of the anhydride absorption of NCA at 1853 cm^{-1} and 1875 cm^{-1} disappeared and the characteristic amide I (1652 cm^{-1} for PCIP**L**G and PCIP**D**G, and 1661 cm^{-1} for PCIP**LD**G) and amide II (1548 cm^{-1}) peaks were detected. The chloride groups were then transferred to the azido groups to afford the polypeptides PAP**X**Gs with the characteristic azido absorption peak at 2099 cm^{-1}. This peak disappeared after reacting with alkyne-functionalized quaternary ammonium salt via copper-catalyzed azide−alkyne cycloaddition (CuAAC) click reactions to afford PTP**X**Gs-TFSI, also called X-50s. Based on the invariance of the absorption peak of amide I, we concluded that the post-modifications implemented do not affect their respective secondary structures. (d) Comparison FTIR spectra of **L**-50, **D**-50 and **LD**-50.

Comparison Group (50%L+50%D): Equimolar mixture of **L**-50 and **D**-50, followed by dissolution in DMF and the drying.

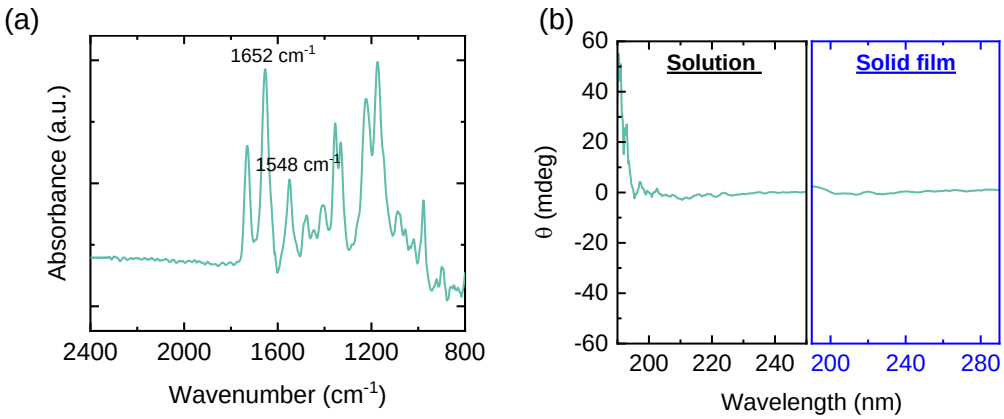

Supplementary Figure 12. (a) ATR-FTIR and (b) CD spectra of equimolar **L**-50 and **D**-50. Helical characteristic amide I peak at around 1652 cm^{-1} was detected, indicating their original helical structure did not disappear after homogeneous mixing. However, despite the helical structure's presence, the CD spectra did not display characteristic double maxima /minima at 208 nm and 222 nm. This is attributed to the formation of a racemic mixture, wherein the optical activity of the two polymer molecules (L-50 and D-50) with opposite directions of helix was canceled out.

3.2 Helical structure stabilizes PPILs

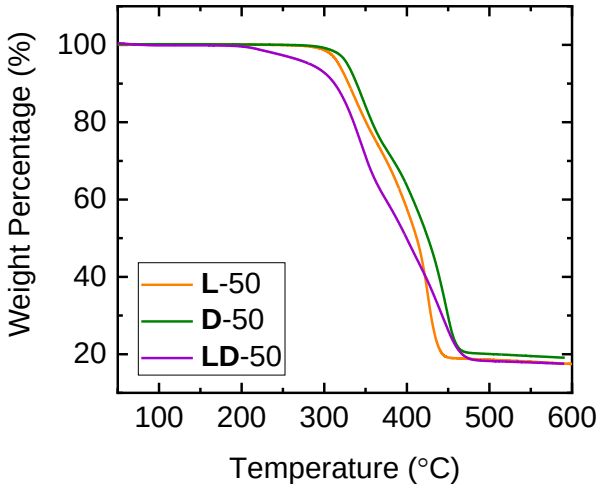

Supplementary Figure 13. TGA spectra of **X**-50s as a function of temperature at a heating rate of 20 °C/min in N_2. The degradation temperatures (T_ds, determined at 5% mass loss): $T_{d,\,L\text{-}50} = 591$ K, $T_{d,\,D\text{-}50} = 598$ K and $T_{d,\,LD\text{-}50} = 556$ K. Helical PPILs showed higher T_d than random coil PPIL, which is attributed to the stability of the helical backbone.

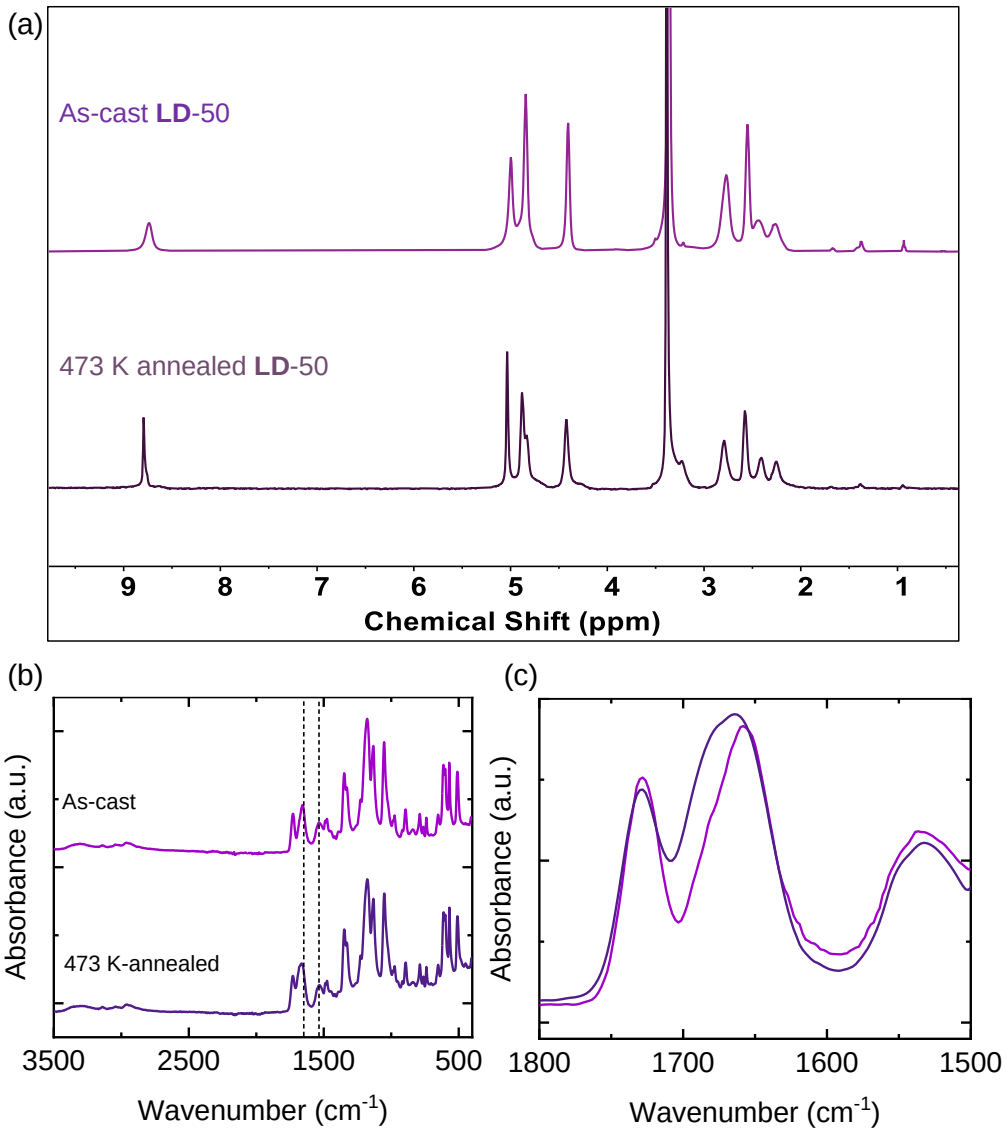

Supplementary Figure 14. (a) stacked ^{1}H-NMR and (b) (c) ATR-FTIR spectra of as-cast and 473K-annealed **LD**-50. No significant changes were observed in the NMR and IR spectra before and after annealing at 473K, except for the broadening of the absorption peak of amide I, indicating no detectable degradation occurred. No obvious changes in helical PPILs.

We attributed this 40 K drop in T_g to a change of H-bonding in random coil structure. Helices are formed and stabilized through intramolecular H-bonding between C=O and N–H groups of the ith and i + 4th residue pair on the same peptide backbone, but random coils do not have any regular H-bonding pattern resulting in less stability.

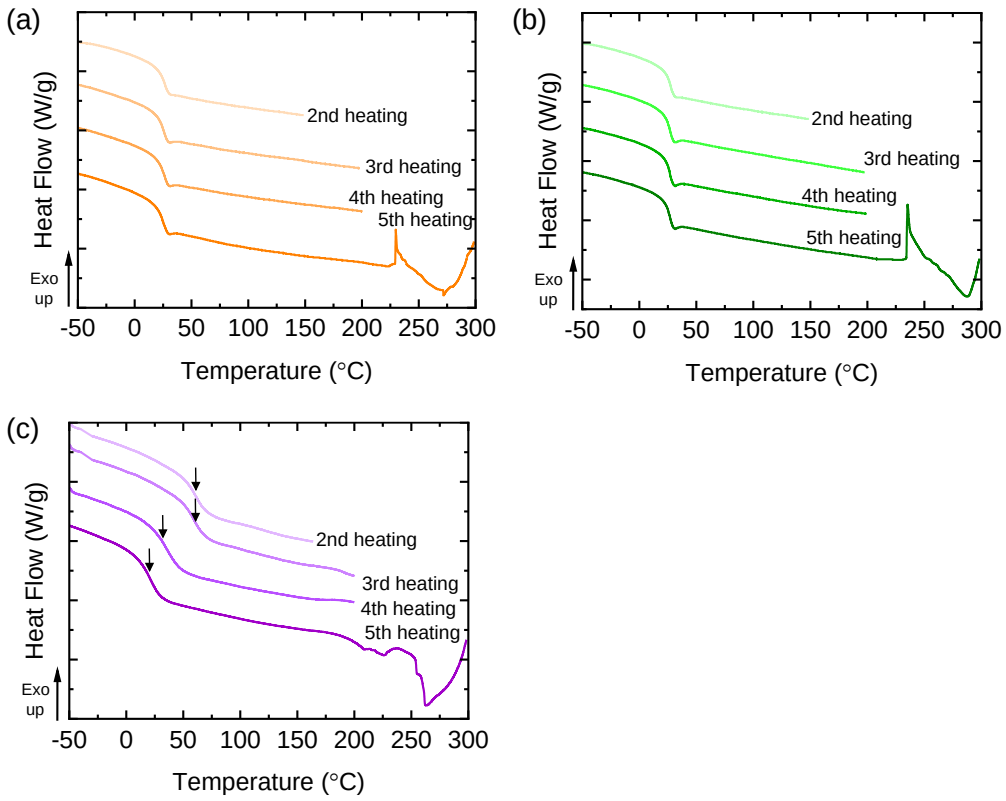

Supplementary Figure 15. DSC profiles of (a) **L**-50, (b) **D**-50 and (c) **LD**-50 with stepwise heating. Step 1: heating from -60 °C to 150 °C and cooling to -60 °C; step 2: heating to 150 °C again and cooling to -60 °C; step 3: heating to 200 °C and cooling to -60 °C; step 4: heating to 200 °C and then cooling to -60 °C; step 5: heating to 300 °C. Heating rate was 10 °C/min.

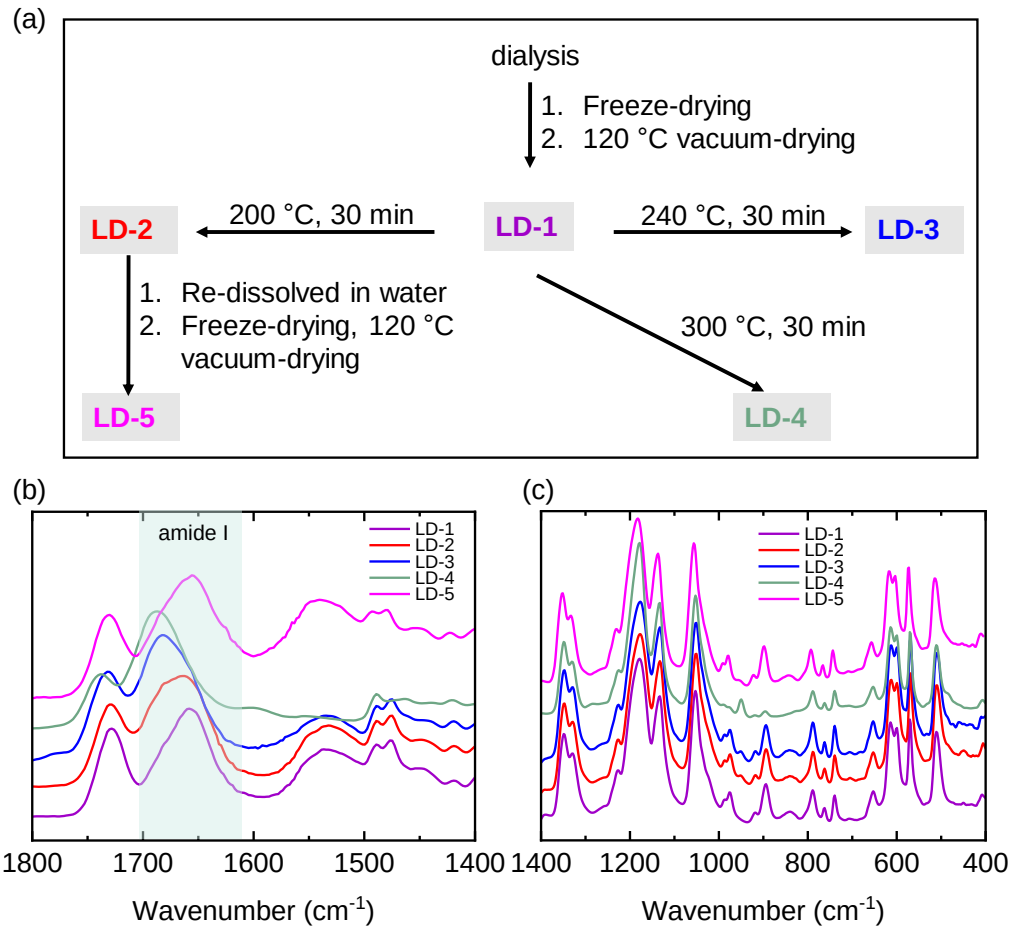

Supplementary Figure 16. (a) Experimental design for studying the thermal transition of random coil **LD**-50 under different annealing temperatures in the glove box. (b) and (c) ATR-FTIR spectra of **LD**-50 with different heat treatments.

LD-1 (purple) represents the as-cast state. Following annealing at 473K (200 °C) for 30 minutes, **LD**-2's (red) amide I peak broadened, while no changes were observed in other peaks. Subsequently, **LD**-2 was dissolved in water and then dried to give **LD**-5 which recovered the narrow amide I peak of **LD**-1. Breaking and rearrangement of unstable H-bonds (relative to the stable intermolecular H-bonds in the helical structure) within the random coil at 473K and be reverted to the original state when redissolved in water. Upon annealing at 513K, **LD**-3's (blue) amide I peak shifted from 1661 cm^{-1} to 1682 cm^{-1}, with no evident changes in other peaks. However, substantial peak variations were detected for **LD**-4 (light green), with the amide I peak shifting to 1688 cm^{-1} and the amide II peak disappearing, indicating thermal degradation.

3.3 Helical structure promotes ionic conductivity

(a)

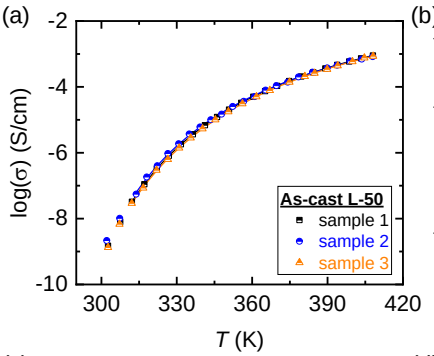

(b)

As-cast **L**-50	T_0 (K)[b]	$T_g - T_0$ (K)	σ_∞ (S/cm)[b]	D[b]
sample 1	249.3	48.3	0.73	4.27
sample 2	251.2	46.4	0.69	4.0
sample 3	247.0	50.6	0.82	4.55

(c)

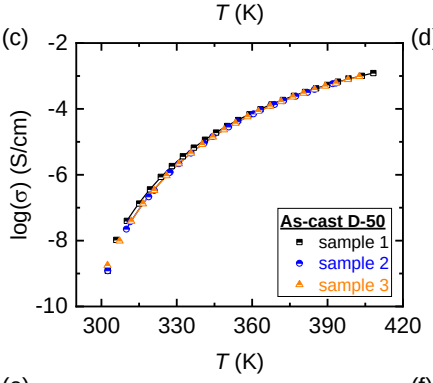

(d)

As-cast **D**-50	T_0 (K)[b]	$T_g - T_0$ (K)	σ_∞ (S/cm)[b]	D[b]
sample 1	249.6	48.1	0.73	4.06
sample 2	251.2	46.5	0.80	4.06
sample 3	251.3	46.4	0.82	4.07

(e)

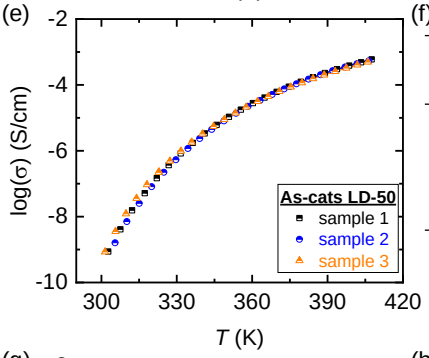

(f)

As-cast **LD**-50	T_0 (K)[b]	$T_g - T_0$ (K)	σ_∞ (S/cm)[b]	D[b]
sample 1	245.6	86.9	1.02	4.91
sample 2	247.1	85.4	0.98	4.82
sample 3	240.3	92.2	1.02	5.26

(g)

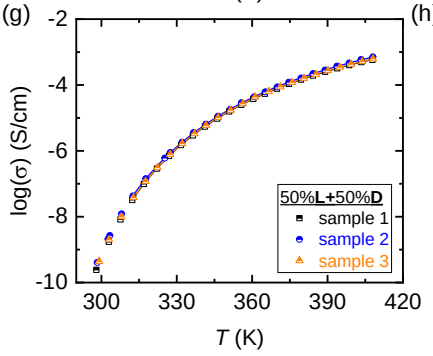

(h)

50%**L**+50%**D**	T_0 (K)[b]	$T_g - T_0$ (K)	σ_∞ (S/cm)[b]	D[b]
sample 1	249.3	48.9	0.40	4.12
sample 2	246.1	52.1	0.48	4.45
sample 3	249.6	48.6	0.39	4.09

Supplementary Figure 17. Ionic conductivity comparisons of as-cast (a) **L**-50, (c) **D**-50, (e) **LD**-50, and (g) 50%**L**+50%**D** as a function of temperature from three independent samples. All solid curves are VFT fits. Tables of VFT fit parameters comparisons of as-cast (b) **L**-50, (d) **D**-50, (f) **LD**-50, and (h) 50%**L**+50%**D** from three independent samples. The average values were used in final analysis (Supplementary Table 2).

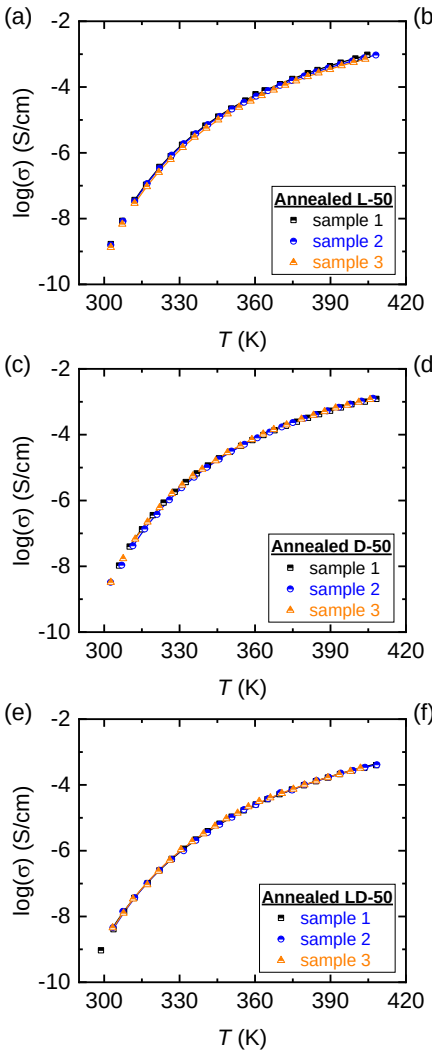

(b)

Annealed **L**-50	T_0 (K)[b]	$T_g - T_0$ (K)	σ_∞ (S/cm)[b]	D[b]
sample 1	249.4	47.9	0.81	4.41
sample 2	249.3	48	0.77	4.27
sample 3	247.5	49.8	0.88	4.51

(d)

Annealed **D**-50	T_0 (K)[b]	$T_g - T_0$ (K)	σ_∞ (S/cm)[b]	D[b]
sample 1	250.9	47.5	0.83	4.09
sample 2	249.7	48.7	0.77	4.21
sample 3	250.4	48.0	0.76	4.02

(f)

Annealed **LD**-50	T_0 (K)[b]	$T_g - T_0$ (K)	σ_∞ (S/cm)[b]	D[b]
sample 1	239.6	52.7	0.48	4.96
sample 2	233.6	58.7	0.42	5.51
sample 3	238.7	53.6	0.53	5.26

Supplementary Figure 18. Ionic conductivity Comparisons of annealed (a) **L**-50, (c) **D**-50 and (e) **LD**-50 as a function of temperature from three independent samples. All solid curves are VFT fits. Tables of VFT fit parameters comparisons of annealed (b) **L**-50, (d) **D**-50 and (f) **LD**-50 from three independent samples. The average values were used in final analysis (Supplementary Table 2).

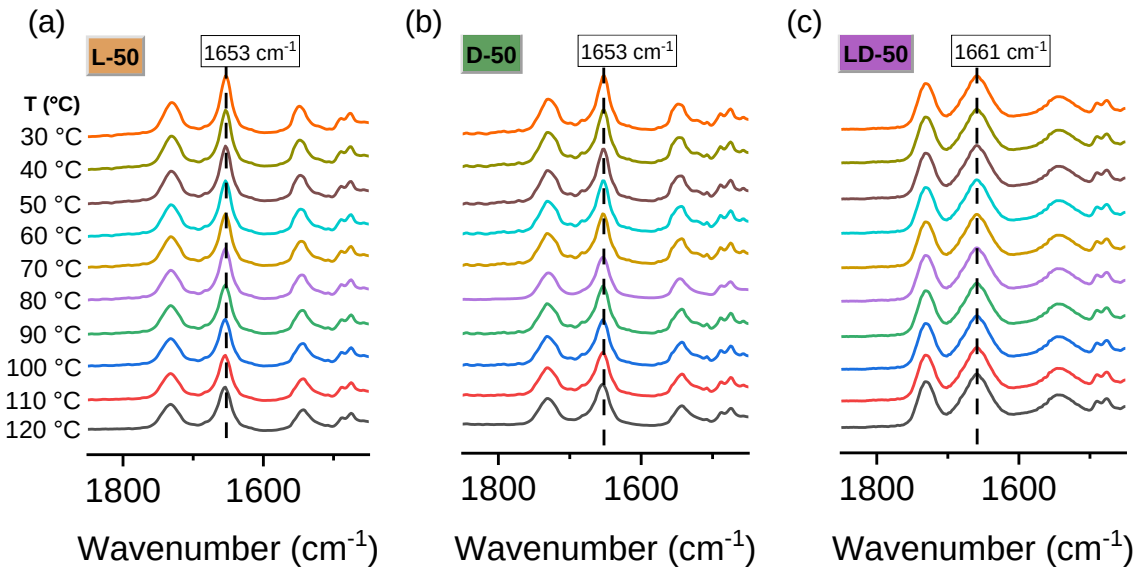

Supplementary Figure 19. Normalized temperature-dependent ATR-FTIR spectra of (a) **L**-50, (b) **D**-50 and (c) **LD**-50 in the region of 1950 cm^{-1} to 1450 cm^{-1}. The invariance of amide I peak indicates the stability of both helix and random coil conformations during ionic conductivity measurements.

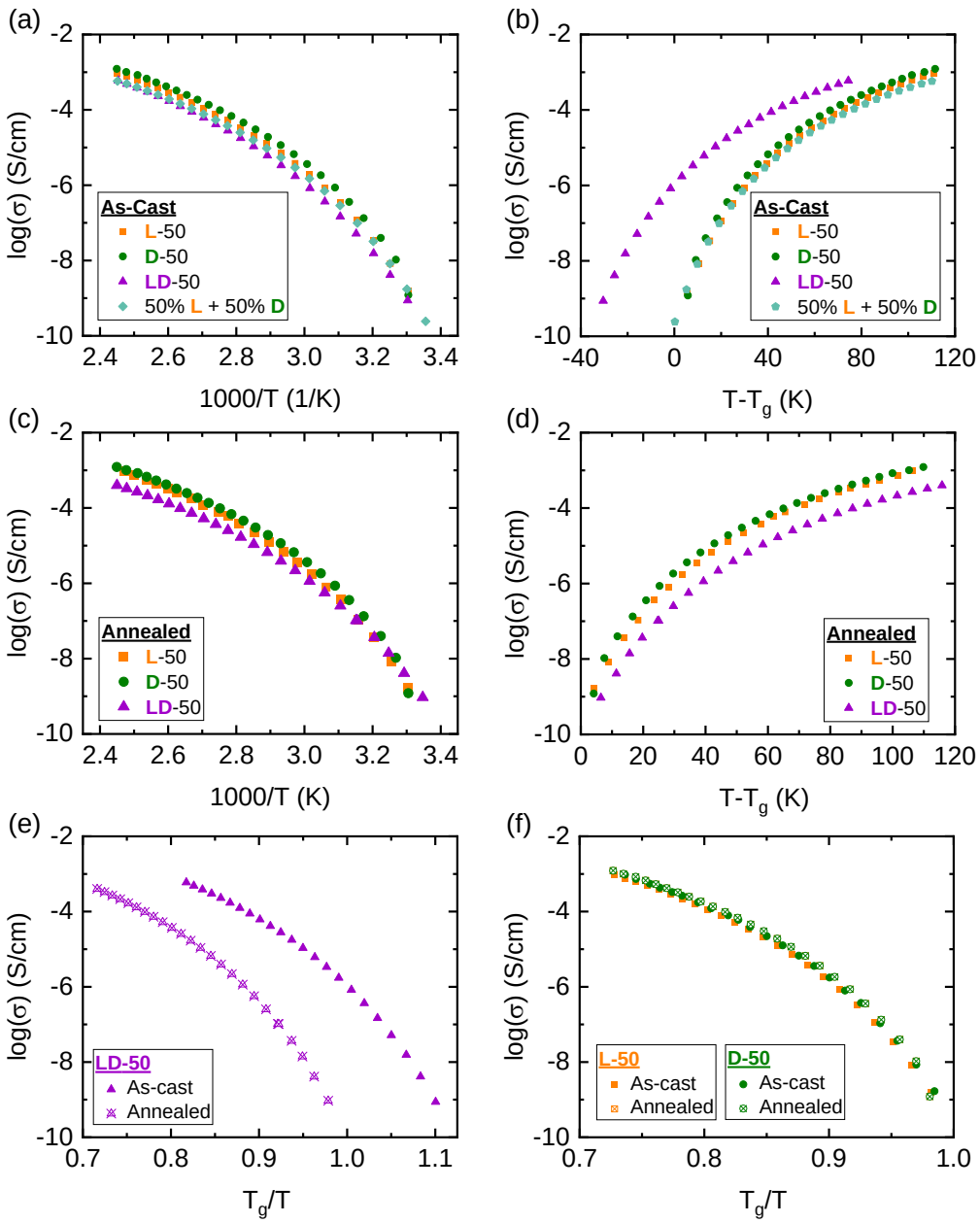

Supplementary Figure 20. Ionic conductivities of as-cast **X**-50s as a function of (a) 1000/T and (b) T-T_g. Ionic conductivities of annealed **X**-50s as a function of (c) 1000/T and (d) T-T_g. T_g-normalized ionic conductivity comparison of as-cast and annealed **X**-50s: (e) **LD**-50 and (f) **L**-50 and **D**-50.

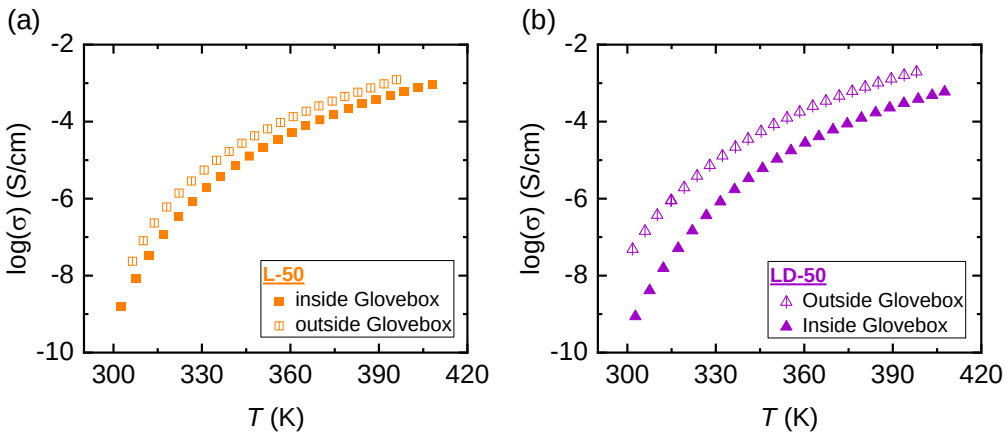

Supplementary Figure 21. The effect of moisture in (a) **L**-50 and (b) **LD**-50 on ionic conductivities. Closed squares and triangles were the ionic conductivities of pre-dried PPILs prepared in glovebox; open squares and triangles were the ionic conductivities of PPILs (pre-exposed to air for one week) prepared outside the glovebox. Under the same condition, moisture has a greater effect on random coil PPIL.

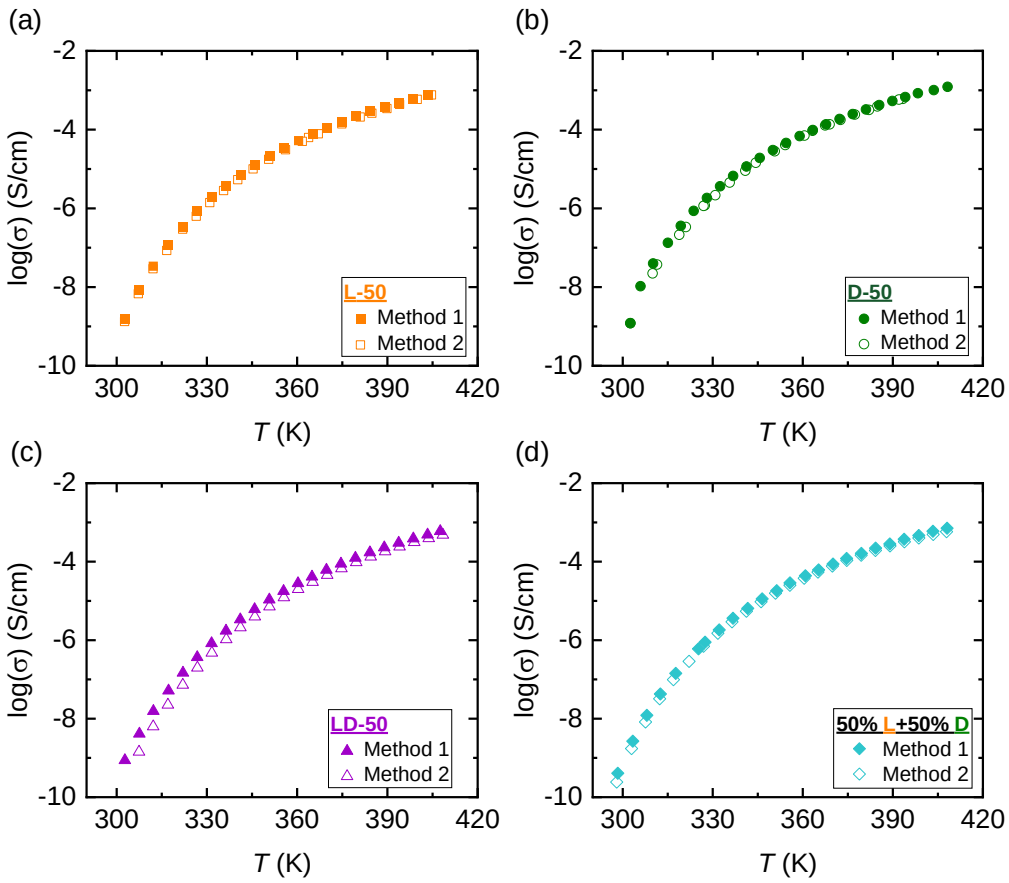

Supplementary Figure 22. Comparison of Ionic conductivities of (a) **L**-50, (b) **D**-50, (c) **LD**-50 and (d) 50% **L**+ 50% **D** by using different measurement methods. Method 1: Data was collected by heating to 140 °C, and measuring ionic conductivity every 5 °C during cooling. Method 2: Data was collected in intervals of 10 °C, first heating to 140 °C and measuring ionic conductivity every during cooling. The samples were heated a second time to 135 °C, and ionic conductivities measured every 10 °C during cooling.

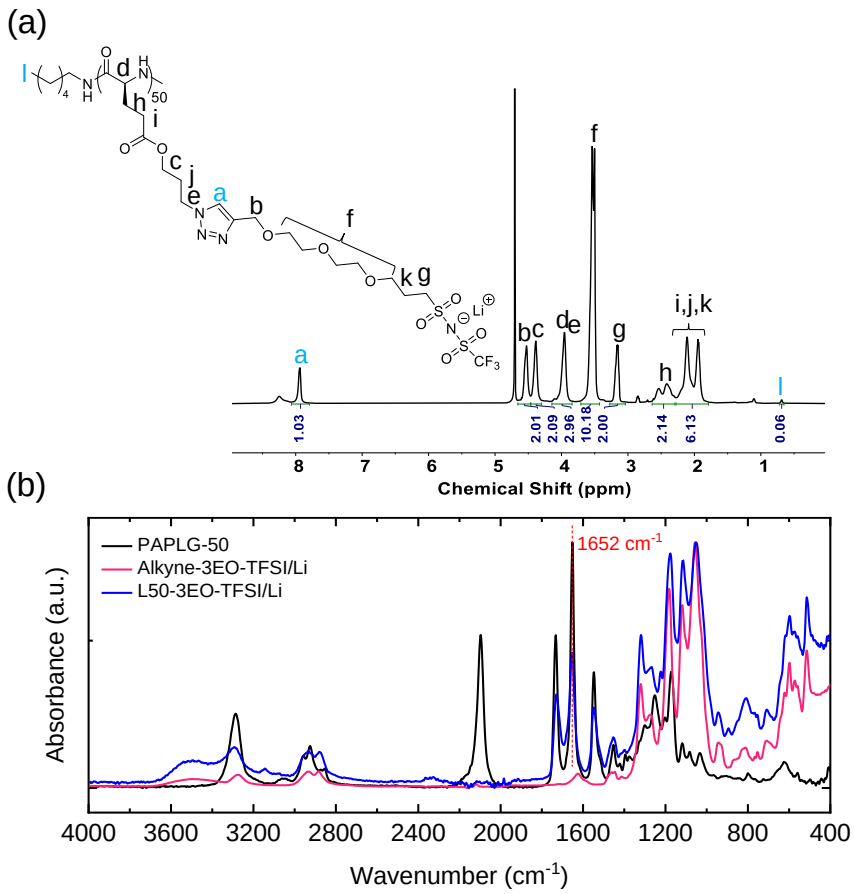

Supplementary Figure 23. (a) ^{1}H-NMR of L50-3EO-TFSI/Li in D_2O. The DP was confirmed to be 50 by the integration ratio of [peak a] and [peak l]. The quantitative conversion of side chain was also confirmed by the integration of [peak a] and [peak g]. (b) ATR-FTIR spectra of alkyne-3EO-TFSI/Li and azide-functionalized PAPLG. Right-handed α helical conformation was confirmed by the characteristic absorbance peaks of amide I at 1652 cm^{-1}.

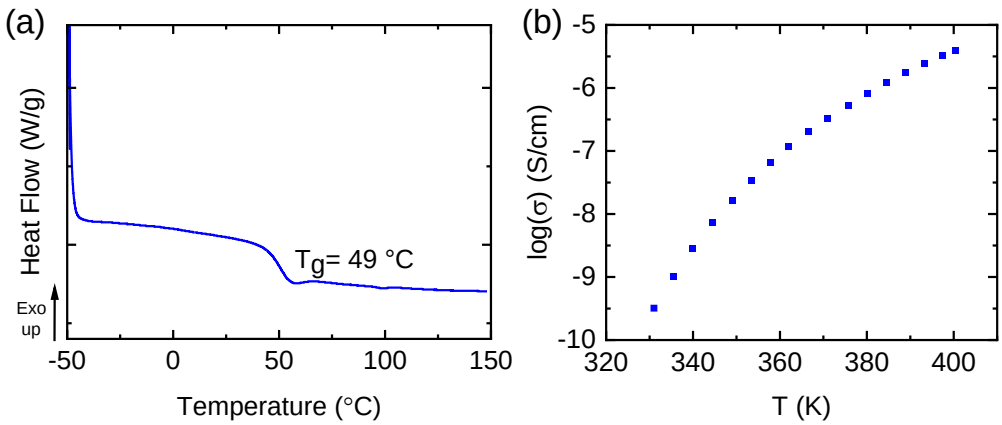

Supplementary Figure 24. (a) Second heating DSC traces and (b) ionic conductivity of single Li conducting polypeptide, L50-3EO-TFSI/Li.

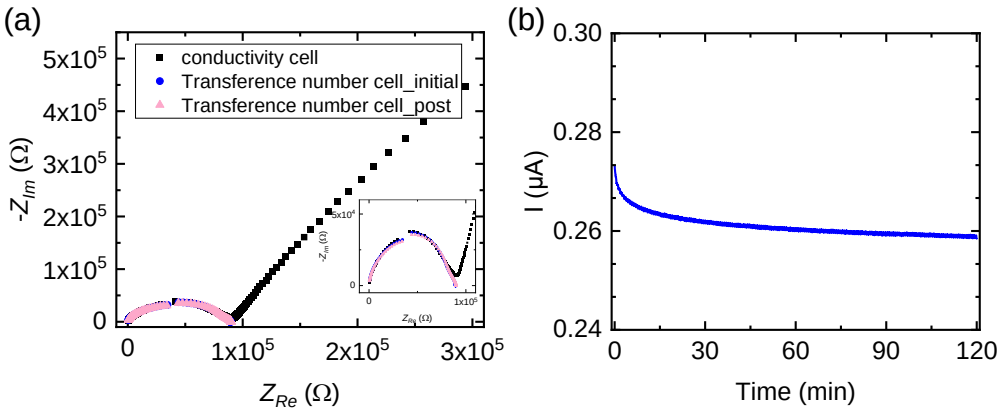

Supplementary Figure 25. (a) Nyquist plots of the impedance measurements before (initial, blue) and after (post, pink) polarization with an amplitude 20 mV. (b) Current vs time profile during the polarization experiment, where 40 mV was applied for 2 hr. All data collected at 100 °C. Three independent cells were produced and showed similar results. A transference number t^{+}_{ss} = 0.93 ± 0.05 was obtained.[6]

3.4 Nanoscale morphology of PPILs

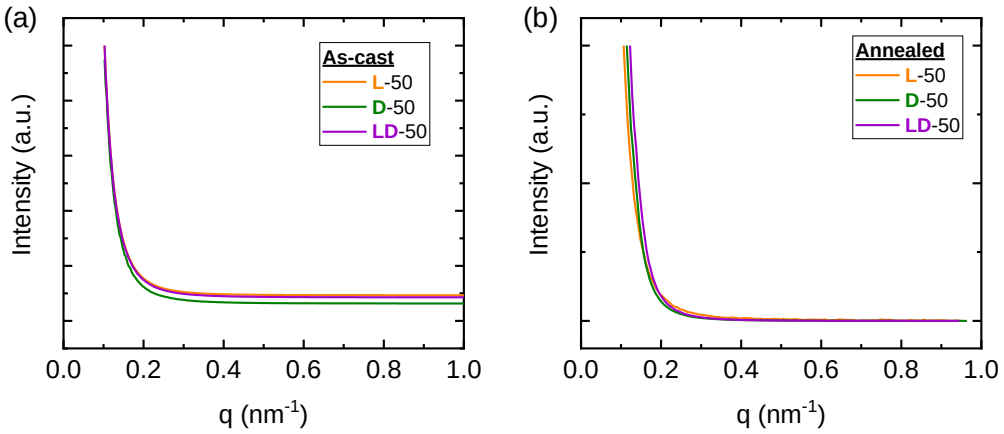

Supplementary Figure 26. Normalized SAXS profiles of as-cast and annealed **X**-50s.

3.5 Synthesis and characterization of helical PPILs with increasing lengths

PCIPLG$_{50}$-NH$_2$ macroinitiator:

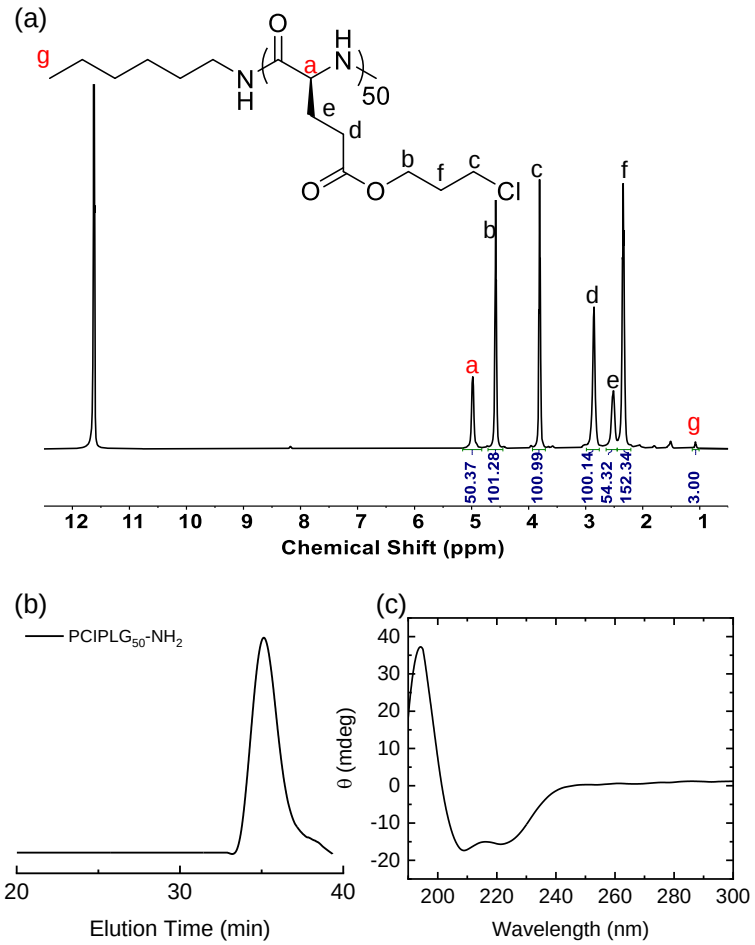

Supplementary Figure 27. (a)^{1}H-NMR, (b) GPC-LS trace and (c) CD spectra of PCIPLG$_{50}$-NH$_2$ macroinitiator. The integration of [peak a] and [peak g, defined as 3] were used to determine the absolute DP** of macroinitiator to be 50. A DP=50 was also obtained based on the M_n=10.26 kDa from SEC. The helical conformation was confirmed by the characteristic absorbance peaks of amide I at 1652 cm^{-1} in FTIR (Supplementary Figure 33a) and the double minima at 208 nm and 222 nm in CD.

(a)

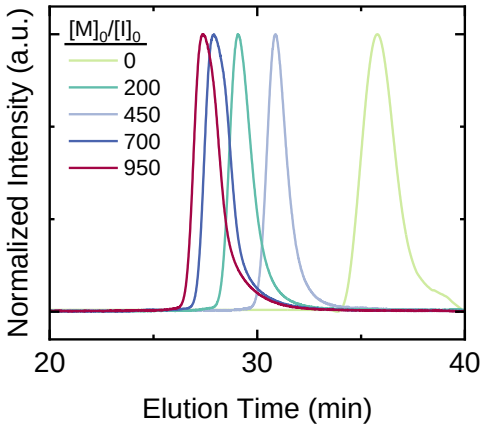

(b)

Polymer	$[M]_0/[I]_0$	M_n (kDa)*	M_w (KDa)*	$Đ$*	DP*
$PCIPLG_{50}$-NH_2	/	10.26	11.09	1.08	50
PCIPLG-233	200	47.8	48.1	1.01	233
PCIPLG-498	450	102.1	103.8	1.02	498
PCIPLG-768	700	157.4	165.1	1.05	768
PCIPLG-925	950	189.6	194.3	1.03	925

Supplementary Figure 28. (a) SEC-LS traces of PCIPLG-DPs initiated by α-helical $PCIPLG_{50}$-NH_2 macroinitiator (I) with crown ether as the catalyst ROP in emulsion system ($V_{DCM}/V_{pH=7\ phosphate\ buffer}$= 95%/5%) with different feeding ratios $[M]_0/[I]_0$. $[M]_0$ = 50 mM. (b) Table of feeding ratios and parameters determined by SEC.

The applicability of ^{1}H NMR end group analysis is constrained by the limitations imposed by high molecular weight, leading to reduced accuracy. However, when comparing the two characterization methods, SEC and NMR, for the three polymers **X**-50s with relatively smaller MW, a remarkable consistency was observed in the obtained DP values. Results obtained through SEC were used to determine the respective DP values for PCIP**L**G-DPs. Additionally, the polypeptide backbones have been confirmed to be stable after post-modification, ensuring that the final PPILs (**L**-DPs) possessed a consistent DP to their respective precursors (PCIP**L**G-DPs).

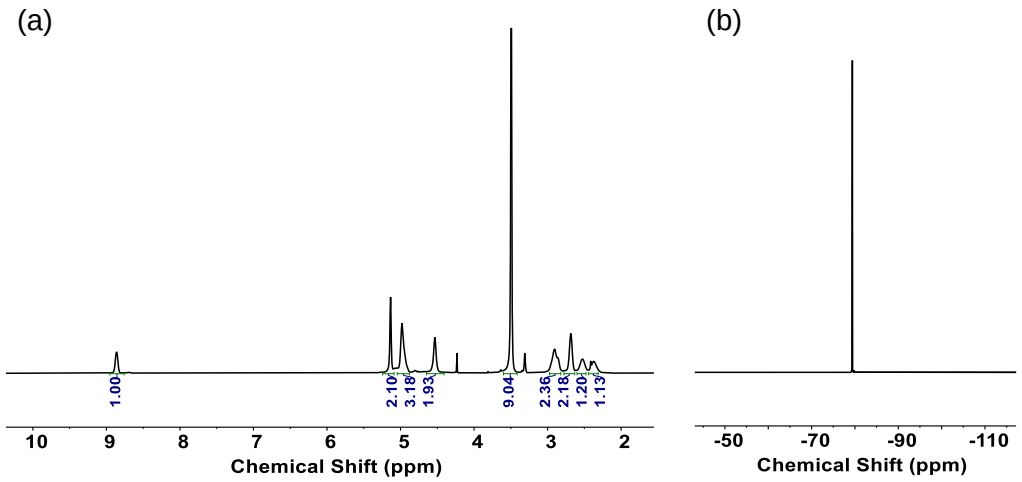

Supplementary Figure 29. (a)^{1}H-NMR and (b) ^{19}F-NMR spectra of **L**-233. ^{1}H-NMR in TFA-*d* and ^{19}F-NMR in DMF-*d*.

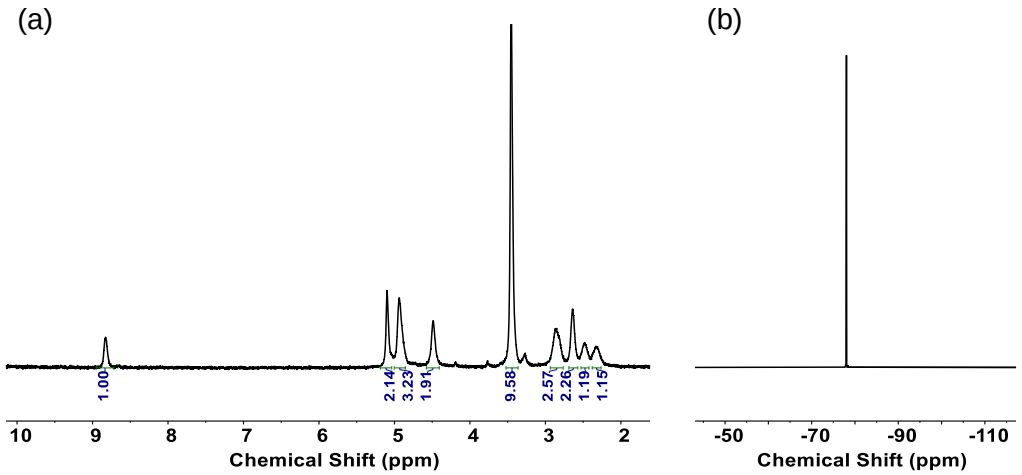

Supplementary Figure 30. (a)^{1}H-NMR and (b) ^{19}F-NMR spectra of **L**-498. ^{1}H-NMR in TFA-*d* and ^{19}F-NMR in DMF-*d*.

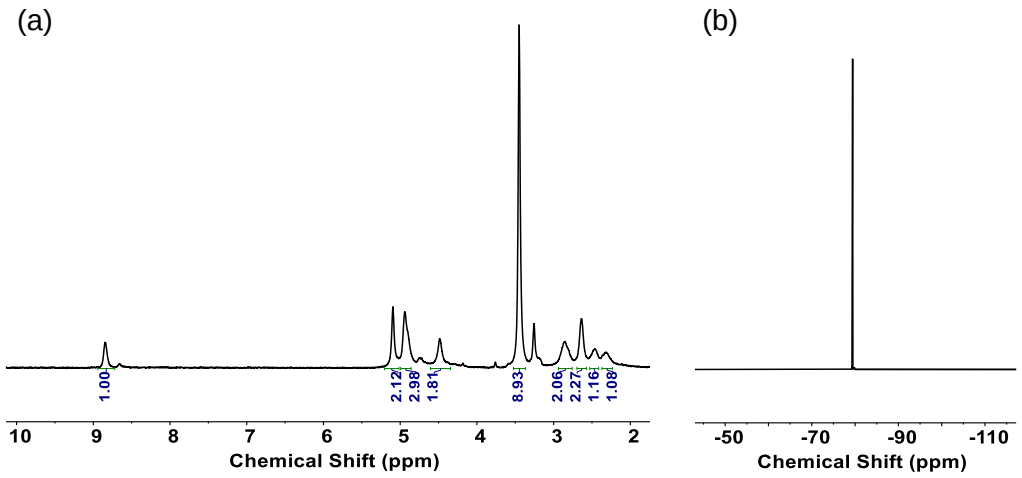

Supplementary Figure 31. (a)^{1}H-NMR and (b) ^{19}F-NMR spectra of **L**-768. ^{1}H-NMR in TFA-*d* and ^{19}F-NMR in DMF-*d*.

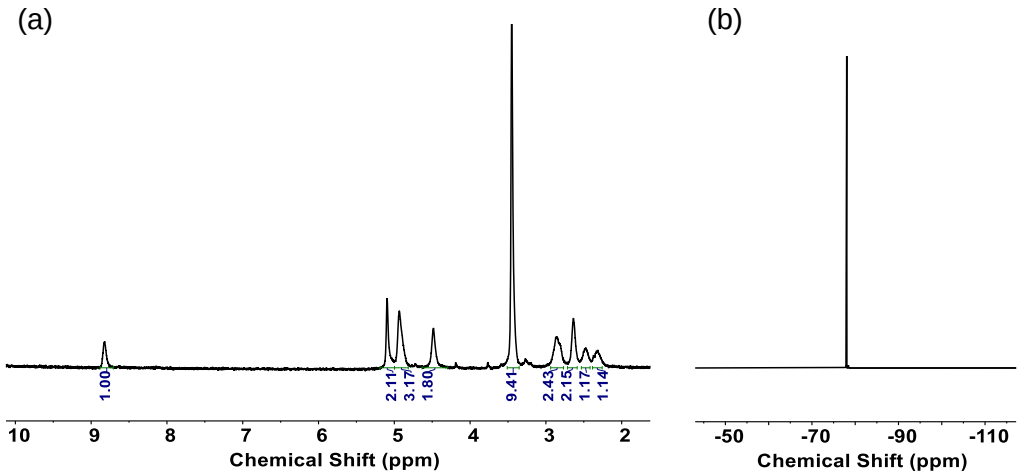

Supplementary Figure 32. (a)^{1}H-NMR and (b) ^{19}F-NMR spectra of **L**-925. ^{1}H-NMR in TFA-*d* and ^{19}F-NMR in DMF-*d*.

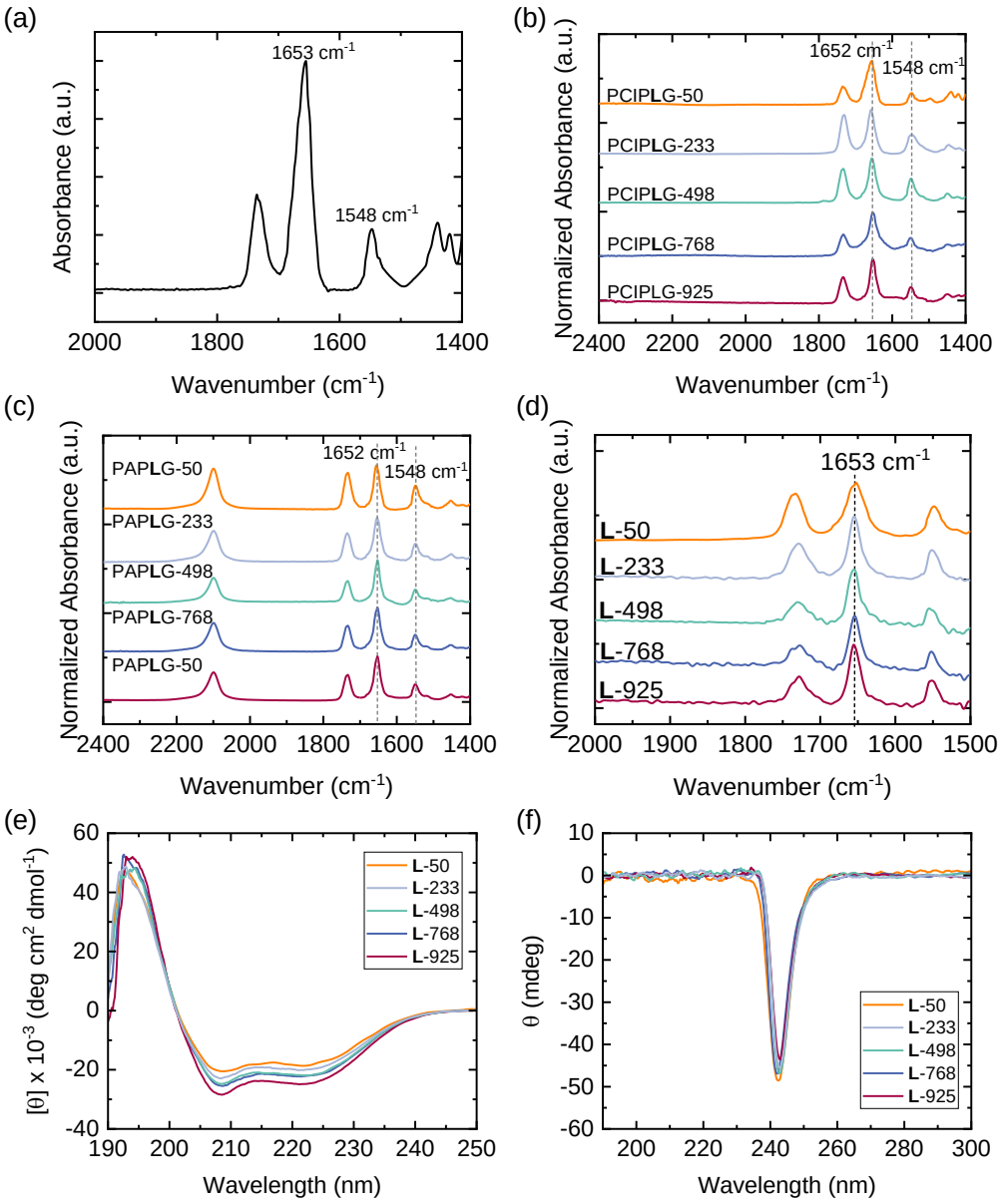

Supplementary Figure 33. FTIR spectra of (a) PCIP**L**G$_{50}$-NH$_2$ macroinitiator, (b) PCIP**L**G-DPs and (c) PAP**L**G-DPs and (d) **L**-DPs. The characteristic amide I (1652-1653 cm^{-1}) and amide II (1548 cm^{-1}) peaks indicate all of them show right-handed α-helical conformations. CD spectra of **L**-DPs in (e) solution phase (in methanol with a concentration of 0.5 mg/mL) and (f) solid films (80 °C hot-pressed solid film, with similar thickness around 100 μm). Both PPILs showed similar characteristic peaks, double-minima at 208 and 222 nm in solution indicating α-helical conformation, and negative peak between 240-250 nm in solid films.

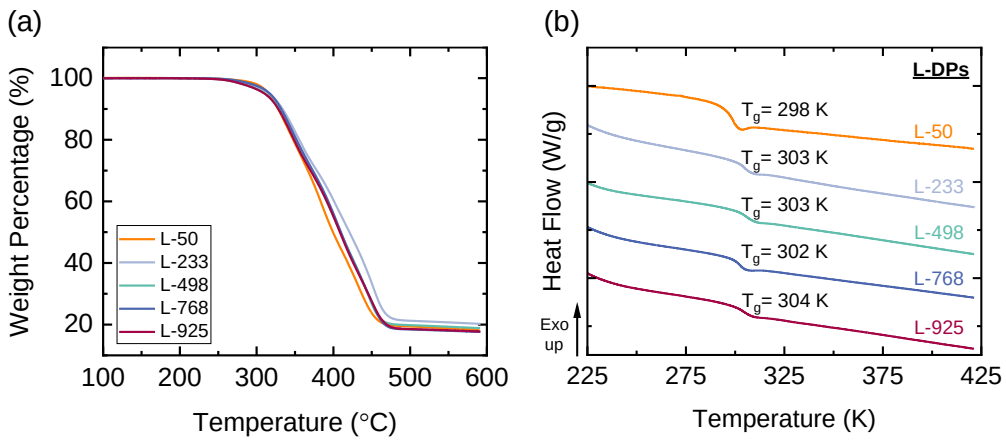

Supplementary Figure 34. (a) TGA spectra of **L**-DPs as a function of temperature at a heating rate of 20 °C/min in N_2. (b) Second heat cycle DSC curves of **L**-DPs under N_2 with heating/cooling scan rate of 10 °C/min.

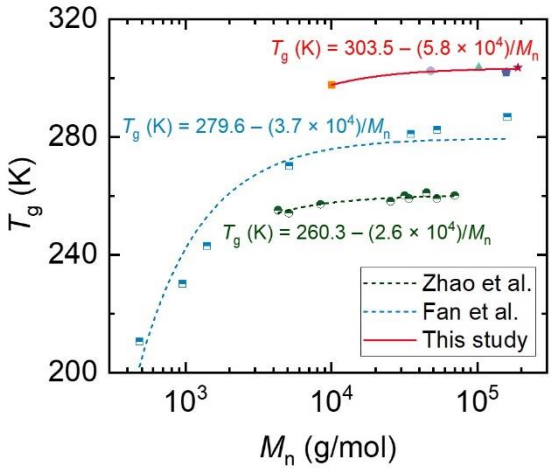

Supplementary Figure 35. The relationship between T_g and M_n of helical PPILs (**L**-DPs), as well as previous studied random coil PILs from Fan et al. (blue)[10] and Zhao et al. (green)[11]. All lines are fit by Fox-Flory Equation T_g (N) = $T_{g,\infty}$ – K/M_n, where $T_{g,\infty}$ is the limiting T_g of polymer with infinite MW and K is a fit parameter relating T_g and DP[12]. The obtained $T_{g,\infty}$ and K values are higher than previously studied random coil PILs[10], due to the rigid helical backbone.

3.6 Longer helices promote higher conductivity

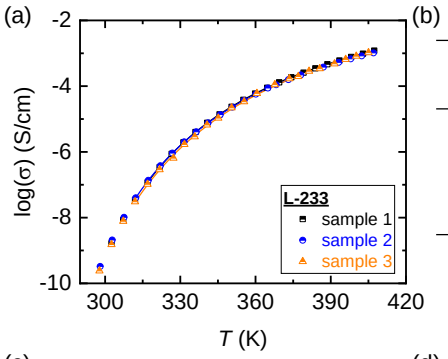

(b)

L-233	T_0 (K)[b]	$T_g - T_0$ (K)	σ_∞ (S/cm)[b]	D[b]
sample 1	247.5	55.0	1.39	4.57
sample 2	246.8	55.7	1.23	4.55
sample 3	248.3	54.2	1.42	4.61

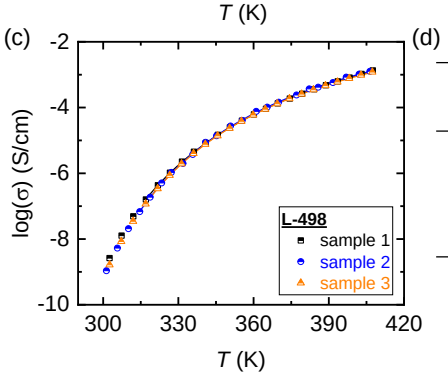

(d)

L-498	T_0 (K)[b]	$T_g - T_0$ (K)	σ_∞ (S/cm)[b]	D[b]
sample 1	239.3	64.1	1.78	4.41
sample 2	246.7	56.7	1.78	4.69
sample 3	247.5	55.9	1.75	4.57

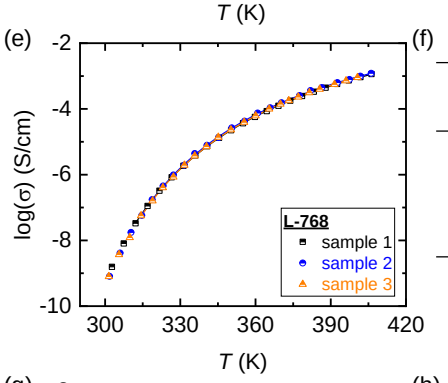

(f)

L-768	T_0 (K)[b]	$T_g - T_0$ (K)	σ_∞ (S/cm)[b]	D[b]
sample 1	246.5	55.5	1.61	4.70
sample 2	251.8	50.2	1.39	4.18
sample 3	249.5	52.5	1.35	4.43

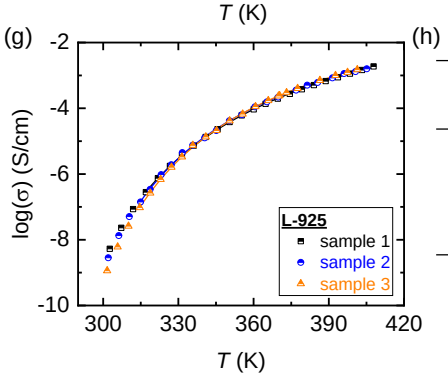

(h)

L-925	T_0 (K)[b]	$T_g - T_0$ (K)	σ_∞ (S/cm)[b]	D[b]
sample 1	243.4	60.2	2.65	5.13
sample 2	248.1	55.5	2.23	5.02
sample 3	250.1	53.5	2.13	5.15

Supplementary Figure 36. Ionic conductivity Comparisons of (a) **L**-233, (c) **L**-498, (e) **L**-768, and (g) **L**-925 as a function of temperature from three independent samples. All solid curves are VFT fits. Tables of VFT fit parameters comparisons of (b) **L**-233, (d) **L**-498, (f) **L**-768, and (h) **L**-925 from three independent samples. The average values were used in final analysis (Supplementary Table 2).

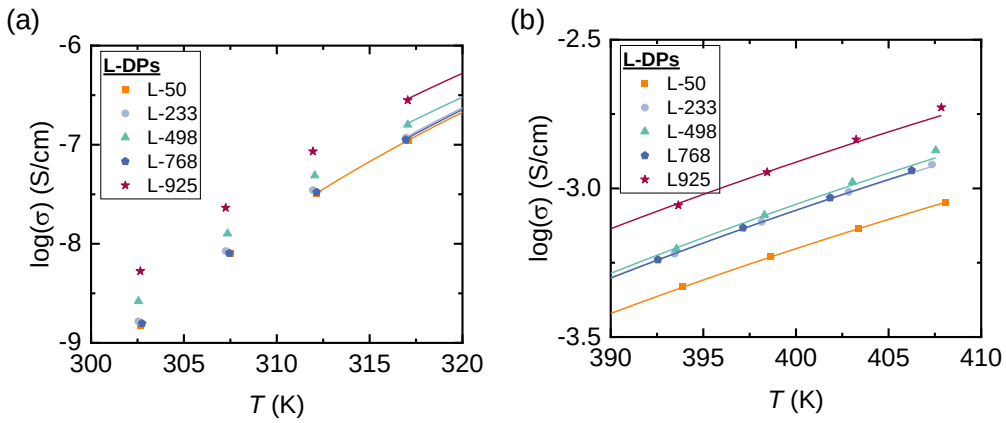

Supplementary Figure 37. Ionic conductivities of **L**-DPs at (a) low temperature and (b) high temperature.

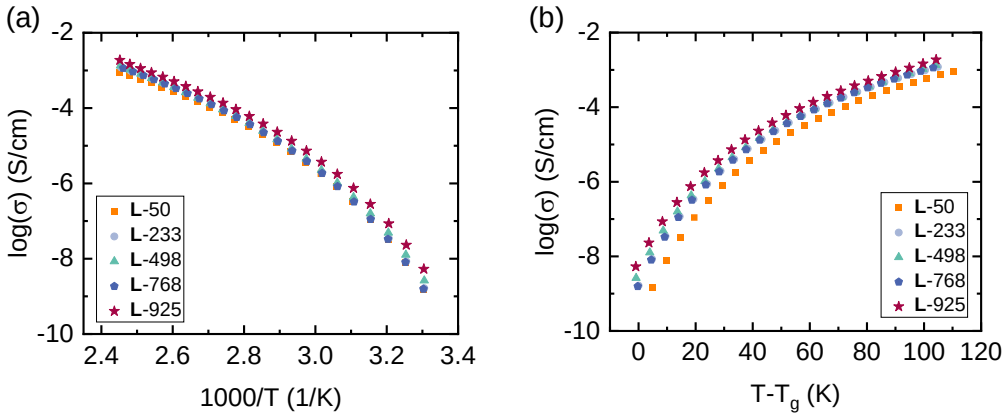

Supplementary Figure 38. Ionic conductivities of **L**-DPs as a function of (a) 1000/T and (b) $T-T_g$.

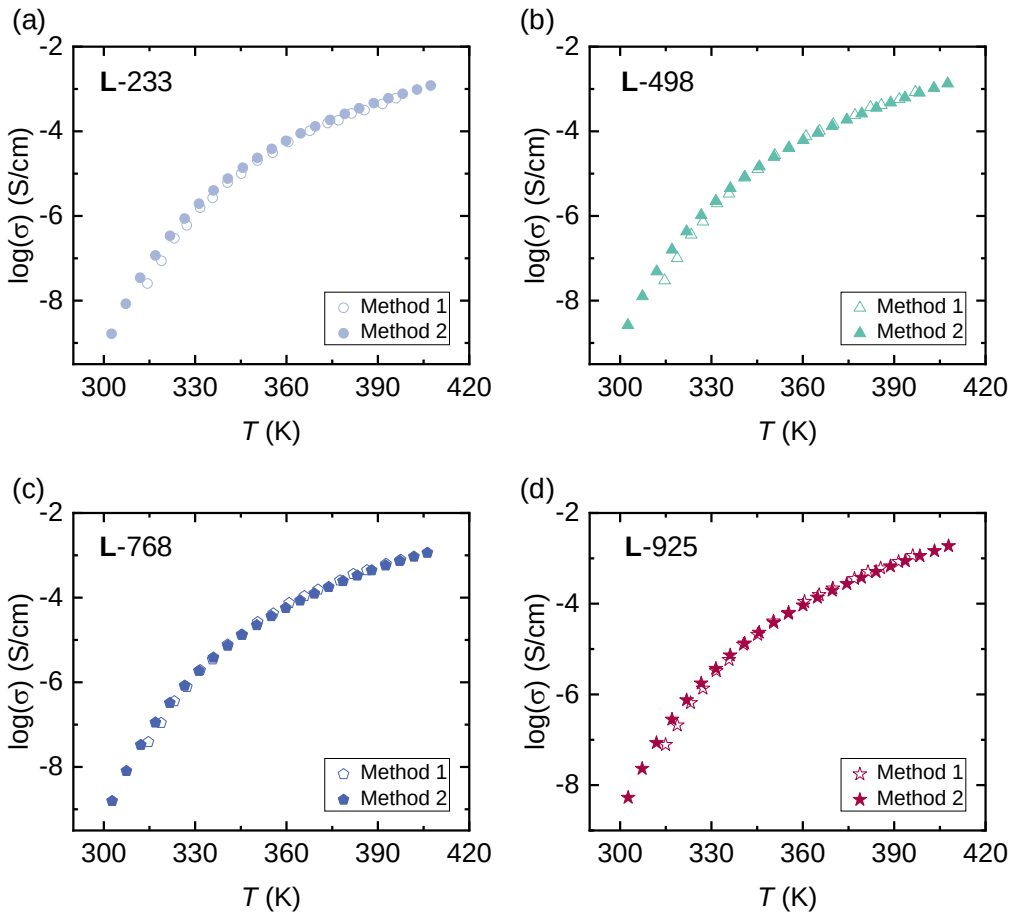

Supplementary Figure 39. Comparison of ionic conductivities of **L**-DPs by using different measurement methods (details in Supplementary Figure 22).

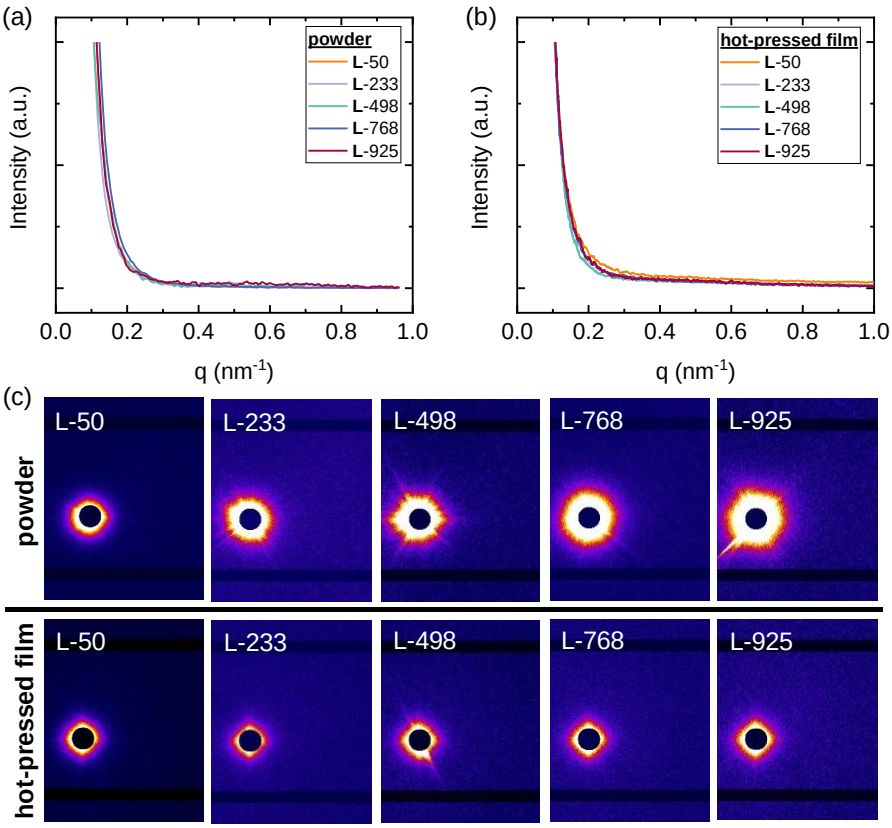

Supplementary Figure 40. Normalized SAXS profiles of L-DPs (a) powder and (b) hot-pressed films. (c) 2D SAXS patterns of L-DPs powder (upper) and hot-pressed films (lower).

3.7 Liquid Crystallinity at PPIL surfaces

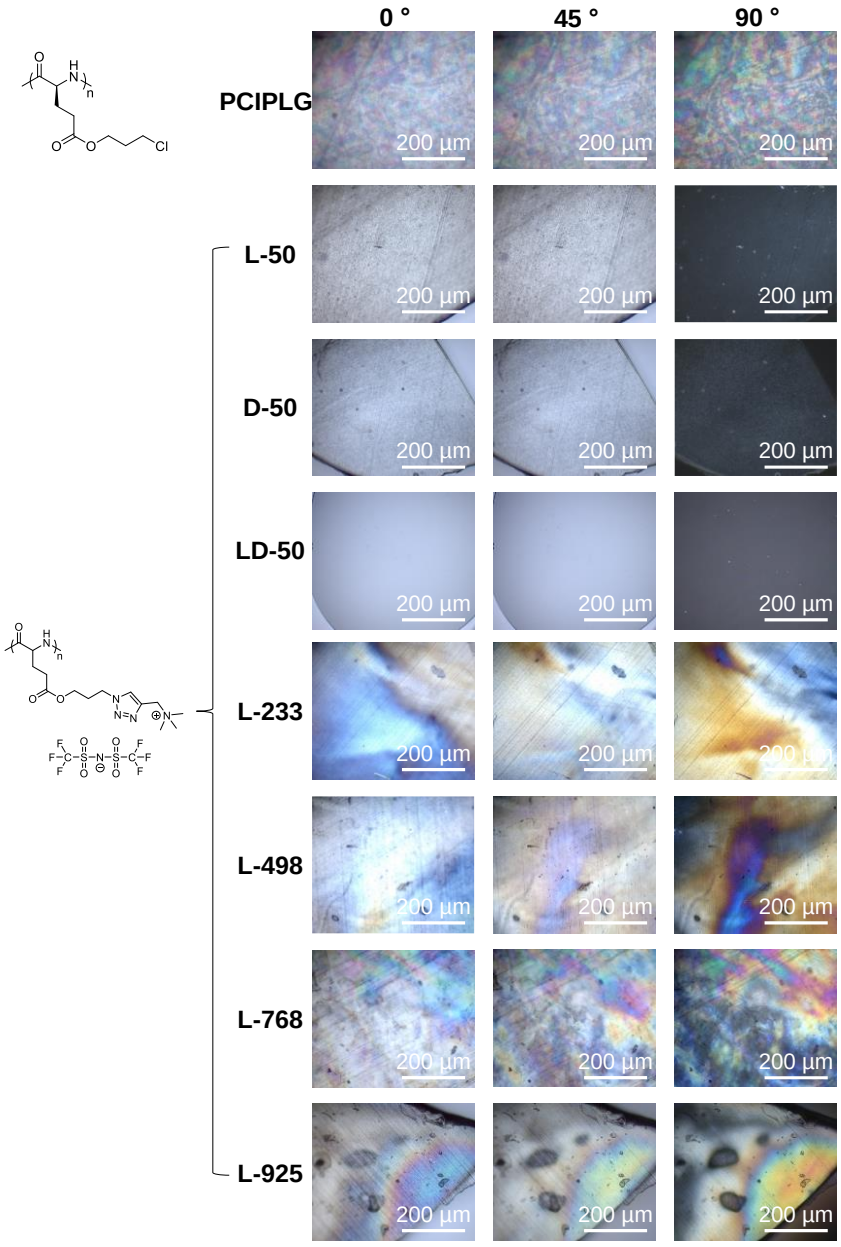

Supplementary Figure 41. POM of helical precursor PCIPLG and **X**-DP hot-pressed films.

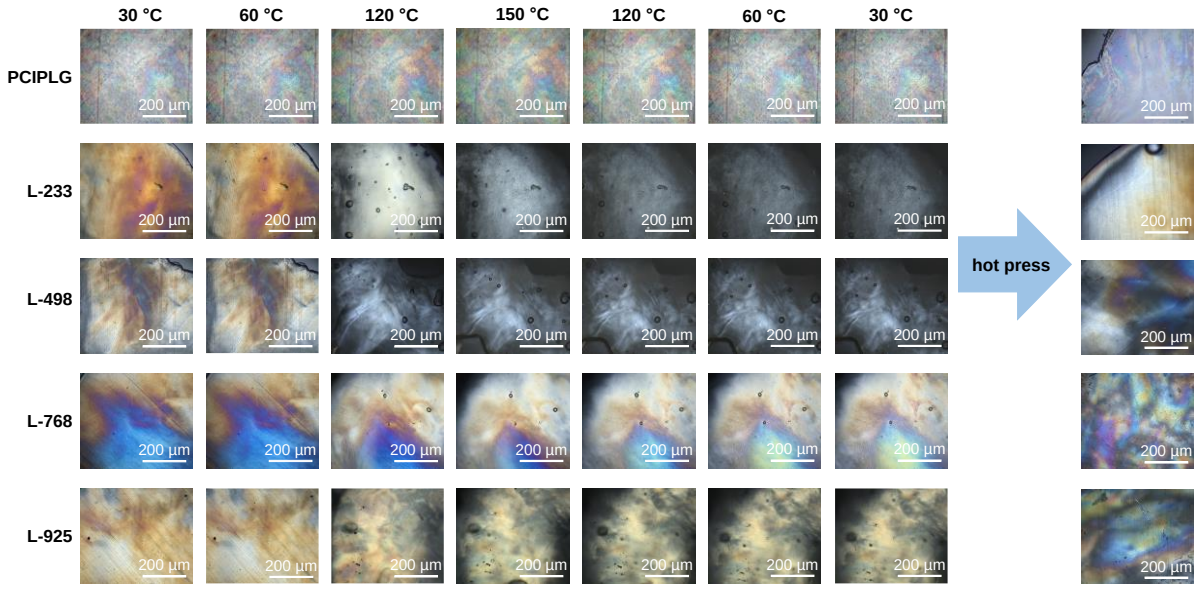

Supplementary Figure 42. The POM images of helical precursor PCIPLG and helical PPILs hot-pressed films with heating and cooling at 10 °C/min.

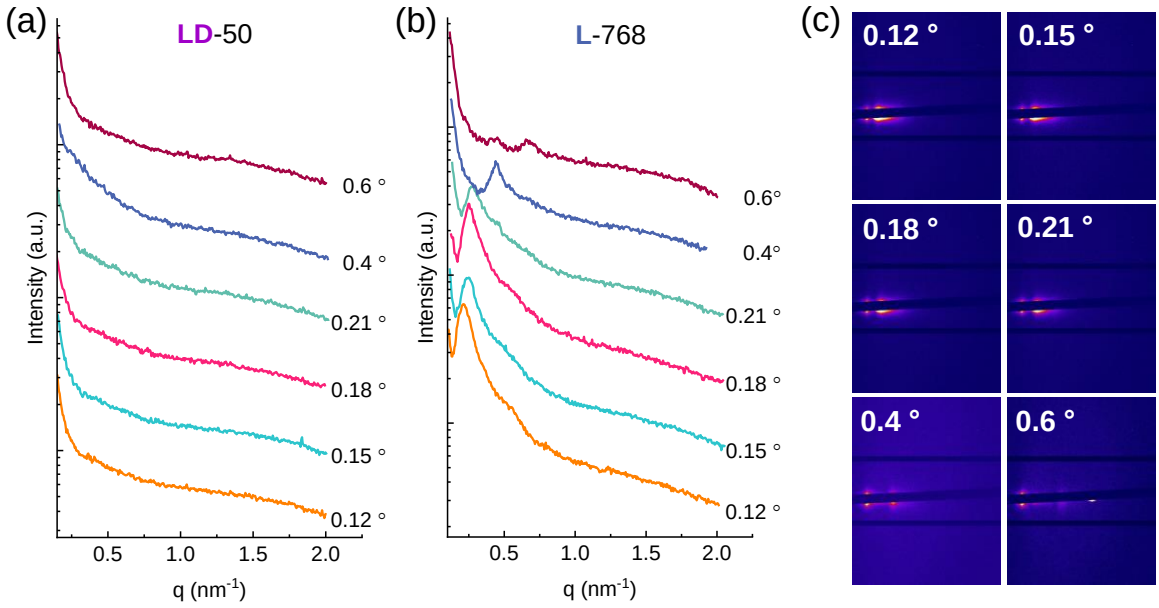

Supplementary Figure 43. (a) GISAXS profiles of (a) LD-50, (b) L-50 and (c) L-768 hot-pressed films with different incidence angles. (d) 2D GISAXS patterns of L-768 hot-pressed film.

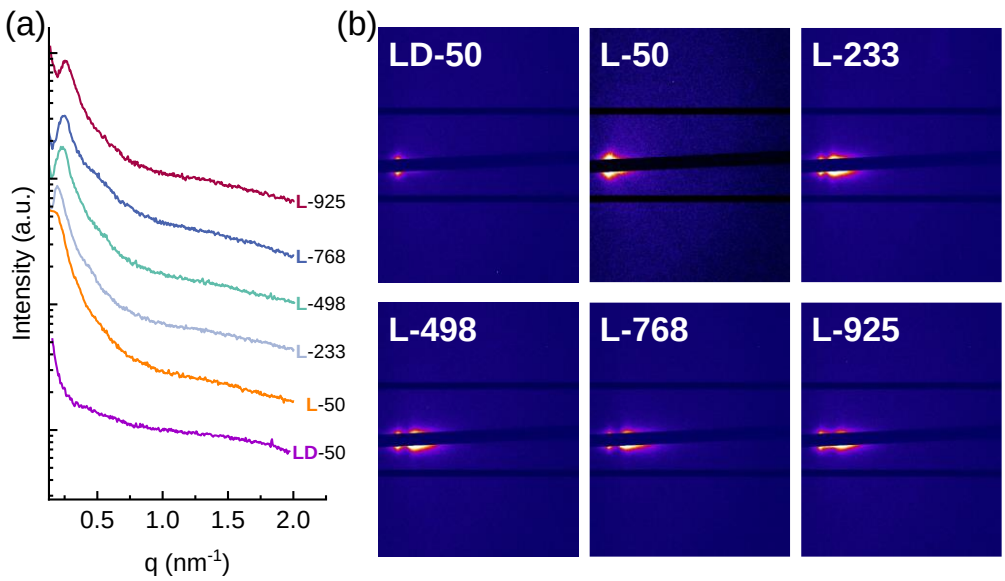

Supplementary Figure 44. (a) GISAXS profiles and (b) 2D GISAXS patterns of L-DPs and LD-50 hot-pressed films at angle of incidence 0.15°.

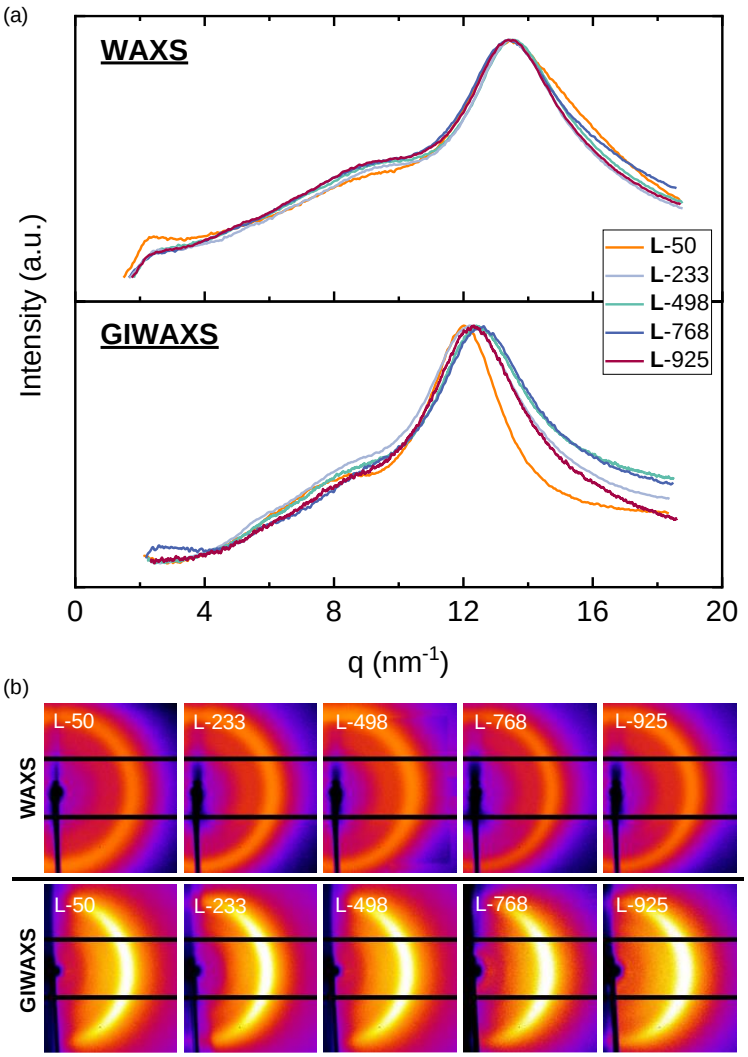

Supplementary Figure 45. Comparisons of (a) profiles and (b) 2D patterns between WAXS and GIWAXS of L-DPs hot-pressed films.

3.8 On-demand Degradation of PPILs

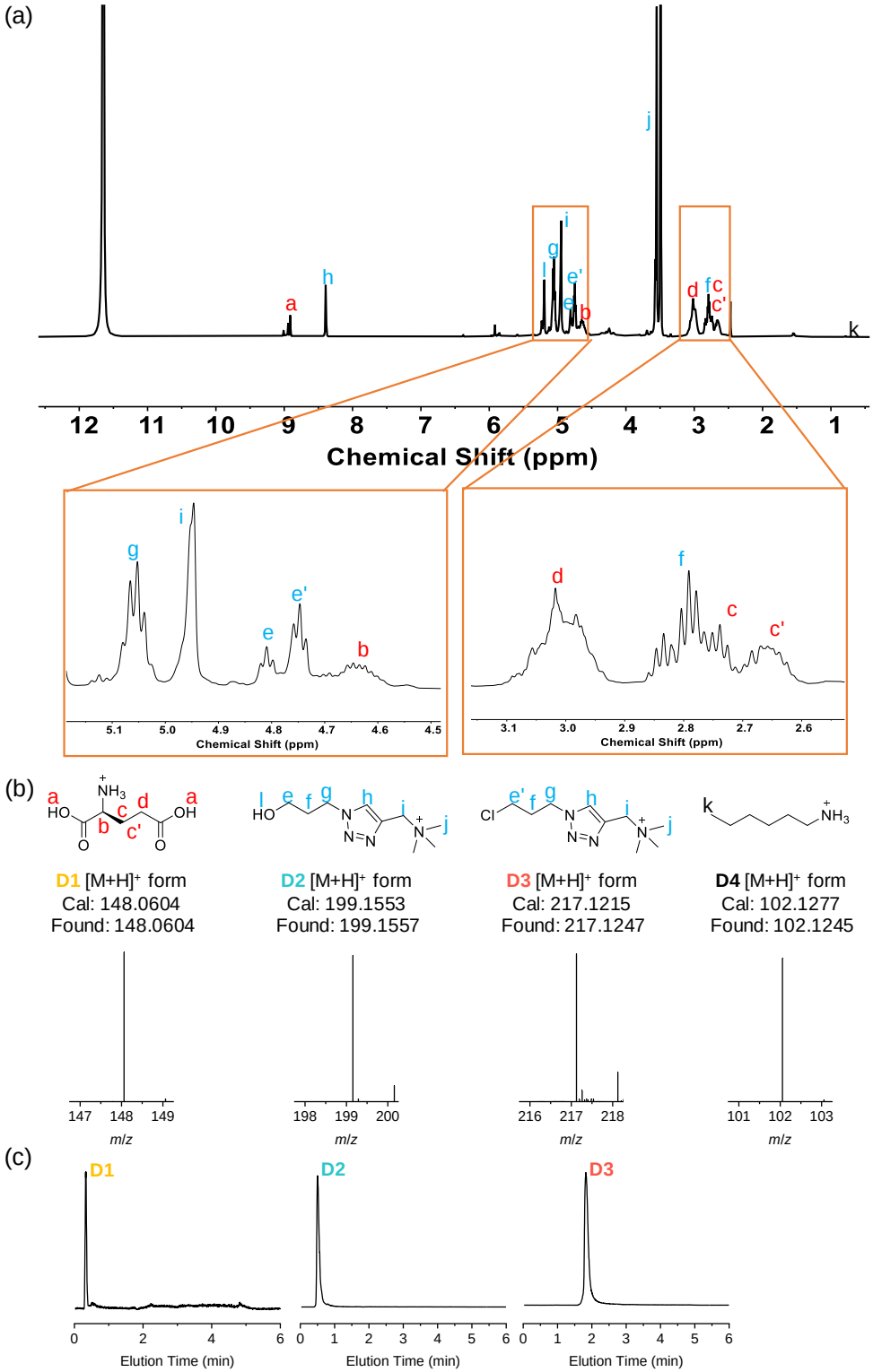

Supplementary Figure 46. Degradation products analysis of **L**-50. (a) ^{1}H-NMR spectra of degraded **L**-50 in TFA-*d*. (b) Chemical structures and molecular weight of observed compounds and (c) their trace maps in LC-MS (positive).

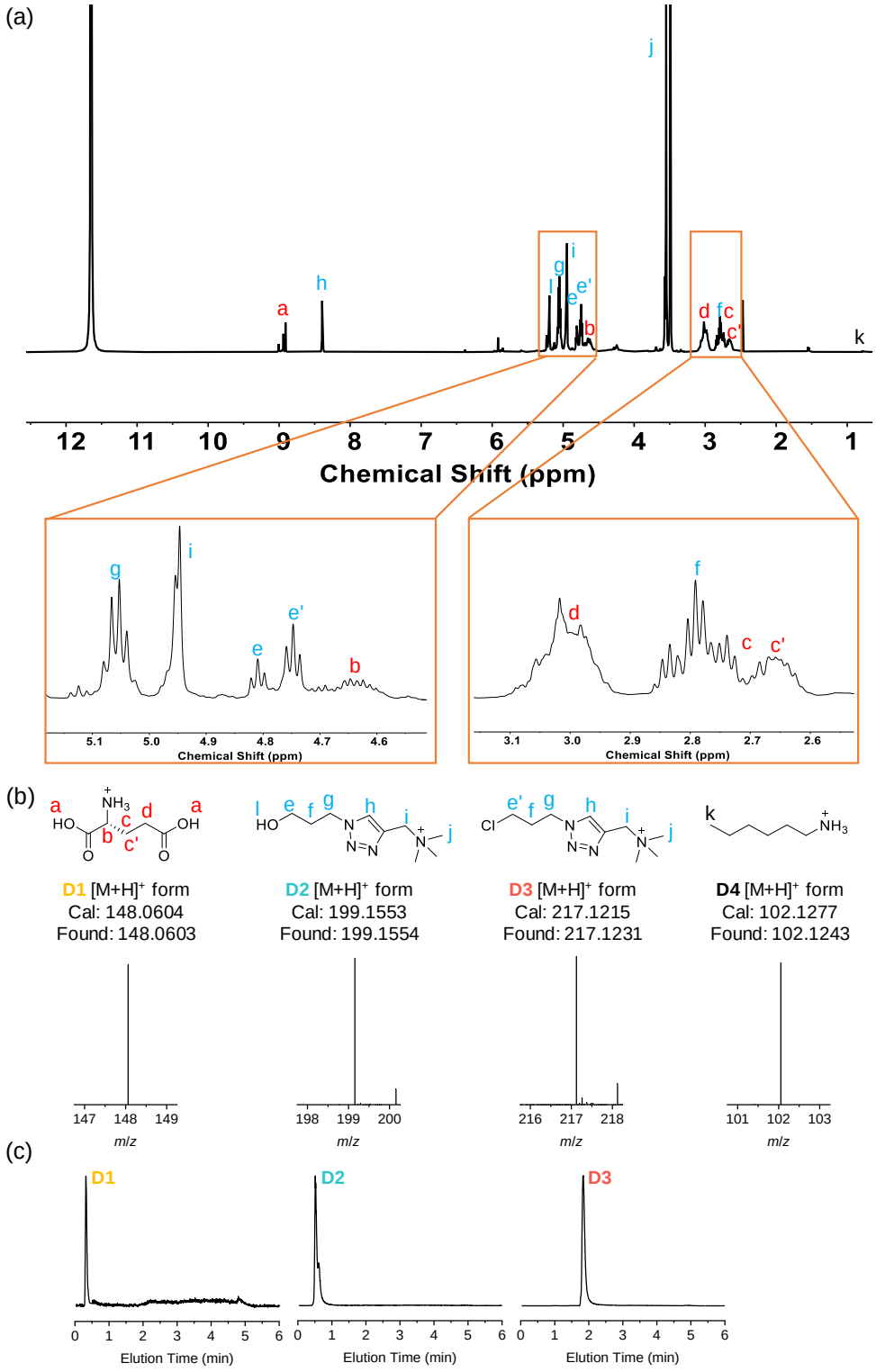

Supplementary Figure 47. Degradation products analysis of **D**-50. (a) ^{1}H-NMR spectra of degraded **D**-50 in TFA-*d*. (b) Chemical structures and molecular weight of observed compounds and (c) their trace maps in LC-MS (positive).

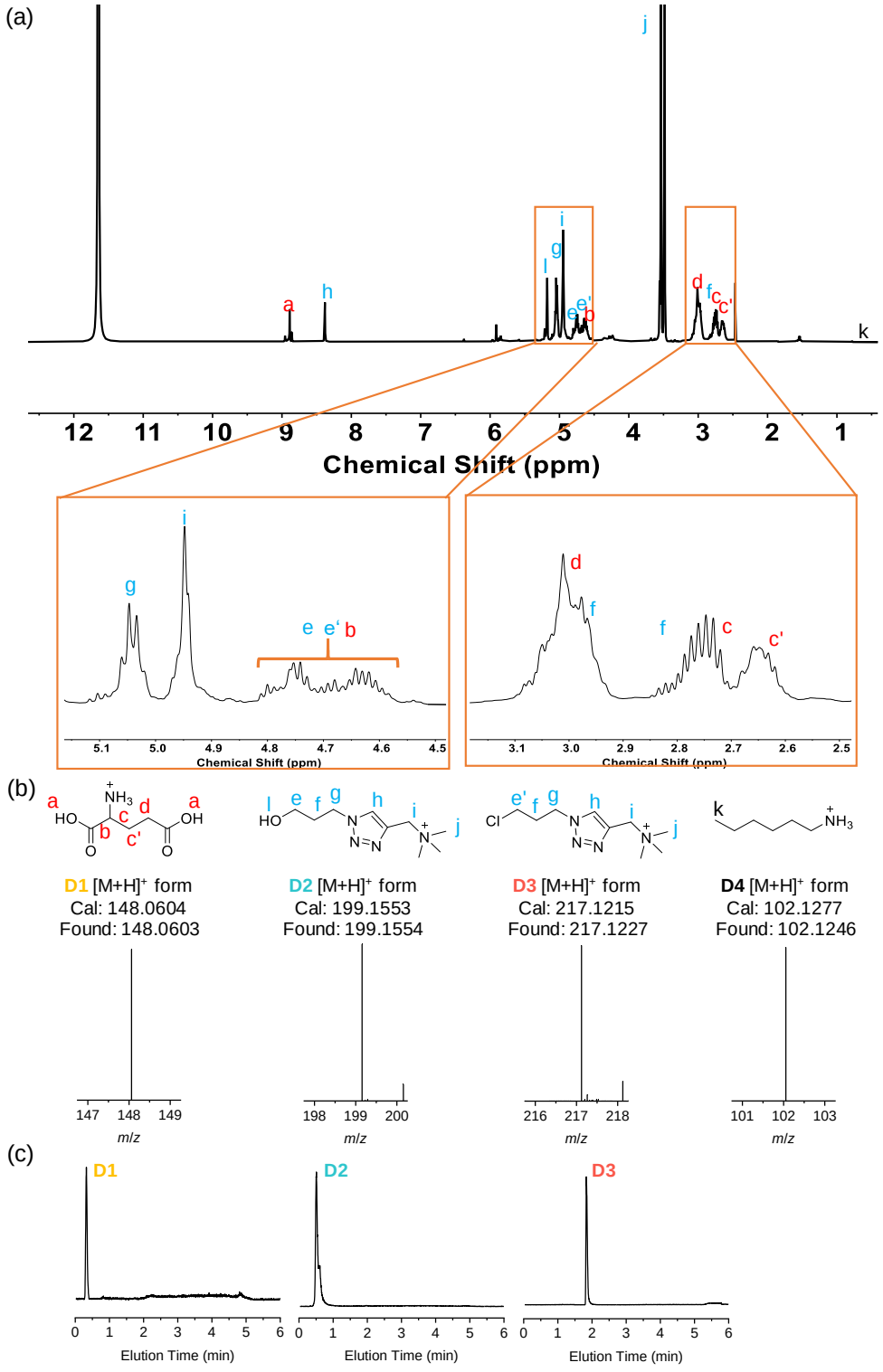

Supplementary Figure 48. Degradation products analysis of **LD**-50. (a) ^{1}H-NMR spectra of degraded **LD**-50 in TFA-*d*. (b) Chemical structures and molecular weight of observed compounds and (c) their trace maps in LC-MS (positive).

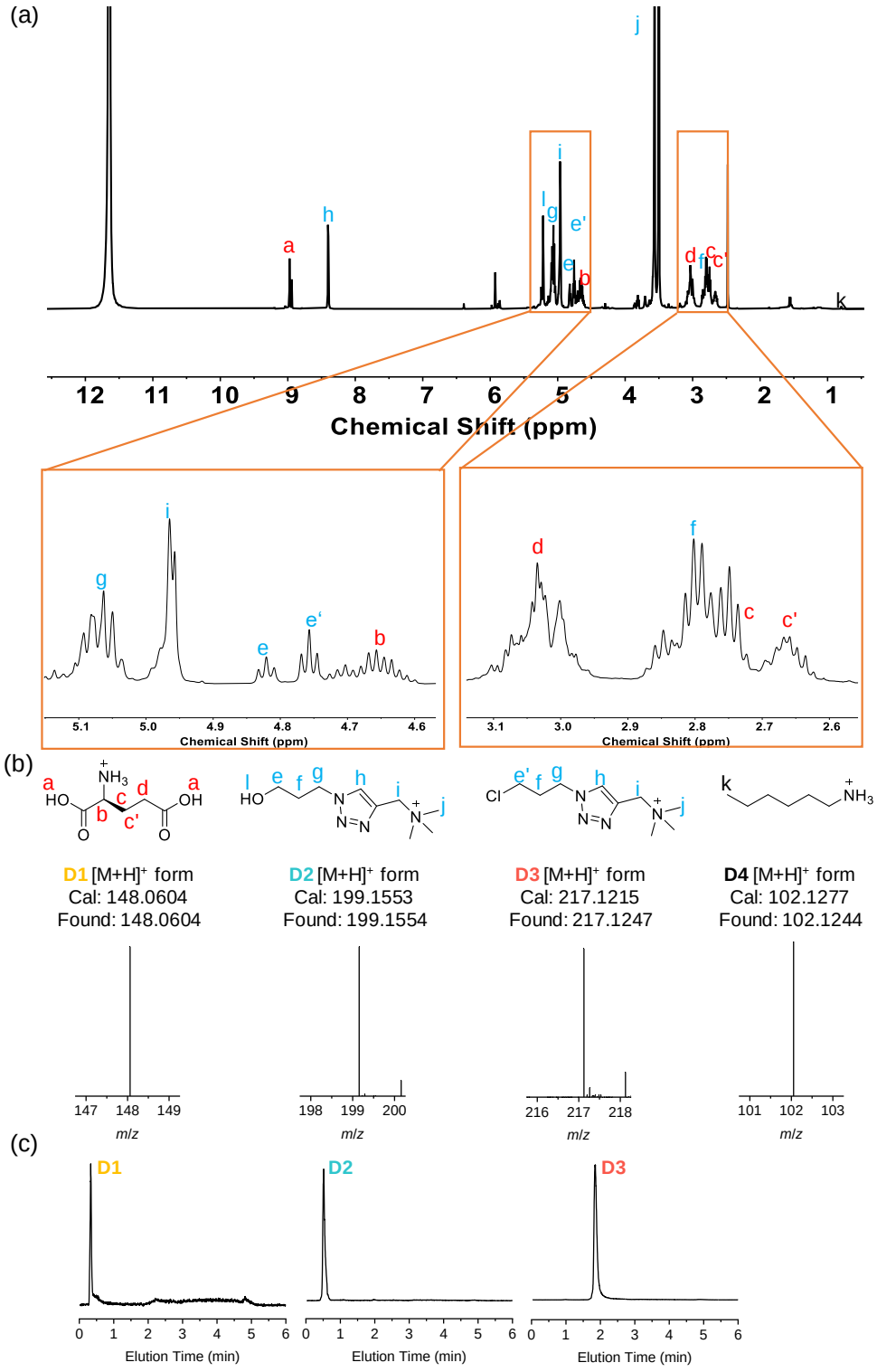

Supplementary Figure 49. Degradation products analysis of **L**-498. (a) ^{1}H-NMR spectra of degraded **L**-498 in TFA-*d*. (b) Chemical structures and molecular weight of observed compounds and (c) their trace maps in LC-MS (positive).

3.9 Cyclic Voltammetry

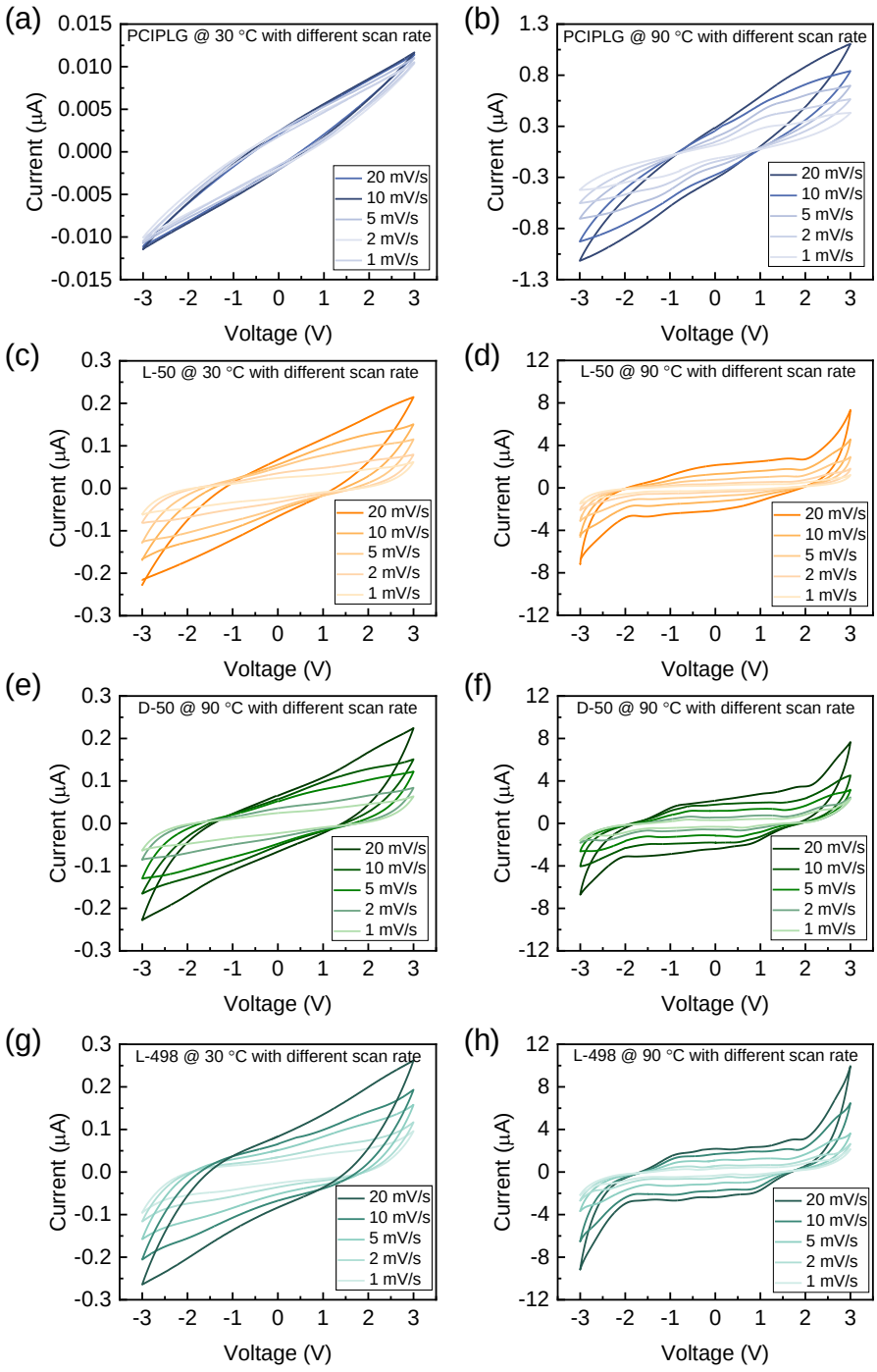

Supplementary Figure 50. Cyclic voltammetry of PCIP**L**G, **L**-50, **D**-50, and **L**-498 with different scan rates at 30 and 90 °C. All samples were tested in three cycles at each scan rate, the curves from each cycle overlapped well. The absence of prominent peaks indicates the stability of the polypeptide precursor and PPILs.

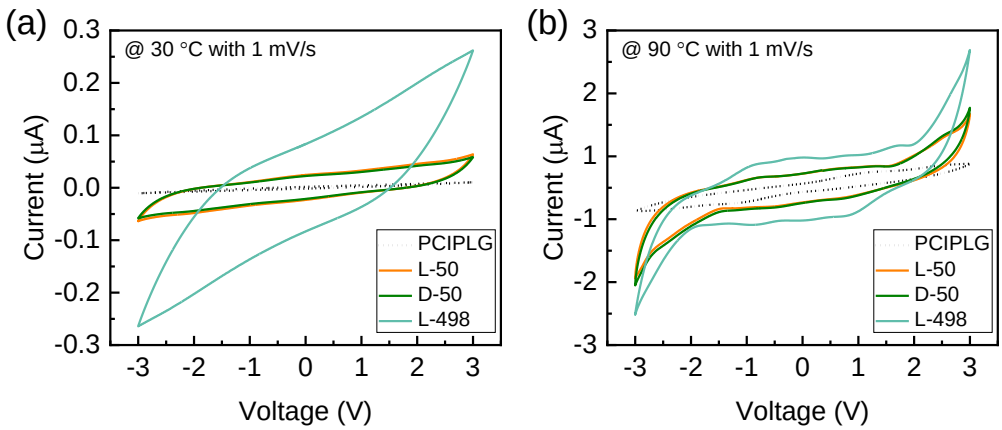

Supplementary Figure 51. Cyclic voltammetry of PCIP**L**G, **L**-50, **D**-50, and **L**-498 when scanned at 1 mV/s at 30 and 90 °C.

Supplementary Table 2. PPILs properties and VFT fit parameters.

Entry	Thermal history	**X**-DPs	*Đ**	IEC[a] (mmol/g)	T_g (k)	T_0[b] (K)	T_g -T_0[b] (K)	σ_∞[b] (S/cm)	D[b]
1	As-cast	**L**-50	1.11	4.87	297 ± 1	249 ± 2	48 ± 2	0.8 ± 0.1	4.3 ± 0.3
2	Annealed	**L**-50	1.11	4.87	297 ± 1	249 ± 1	48 ± 1	0.8 ± 0.1	4.4 ± 0.1
3	As-cast	**D**-50	1.10	4.87	298 ± 1	251 ± 1	47 ± 1	0.8 ± 0.1	4.1 ± 0.1
4	Annealed	**D**-50	1.10	4.87	298 ± 1	250 ± 1	48 ± 1	0.8 ± 0.1	4.1 ± 0.1
5	As-cast	**LD**-50	1.08	4.87	333 ± 2	244 ± 3	88 ± 3	1.0 ± 0.2	5.0 ± 0.2
6	Annealed	**LD**-50	1.08	4.87	292 ± 2	237 ± 3	55 ± 3	0.5 ± 0.1	5.2 ± 0.3
7	As-cast	**L**+**D**	/	4.87	298 ± 1	248 ± 2	50 ± 2	0.4 ± 0.1	4.2 ± 0.2
8	As-cast	**L**-233	1.01	4.87	302 ± 1	248 ± 1	55 ± 1	1.4 ± 0.1	4.6 ± 0.1
9	As-cast	**L**-498	1.02	4.87	303 ± 1	245 ± 4	59 ± 4	1.8 ± 0.1	4.5 ± 0.3
10	As-cast	**L**-768	1.05	4.87	302 ± 1	249 ± 3	53 ± 3	1.5 ± 0.1	4.4 ± 0.3
11	As-cast	**L**-925	1.03	4.87	304 ± 1	247 ± 3	56 ± 3	2.3 ± 0.3	5.1 ± 0.1

* DP and *Đ* were determined by SEC analysis. [a] Theoretical ion exchange capacity (IEC) calculated from molecular formula. [b] VFT fit parameters from three independent samples (Average ± standard error, n = 3). **L**+**D** = 50% **L** + 50% **D**.

4. Reference

1 Tang, H. Y. & Zhang, D. H. General route toward side-chain-functionalized alpha-helical polypeptides. *Biomacromolecules* **11**, 1585-1592, doi:10.1021/bm1002174 (2010).

2 Tang, H., Yin, L., Kim, K. H. & Cheng, J. Helical Poly(arginine) Mimics with Superior Cell-Penetrating and Molecular Transporting Properties. *Chem. Sci.* **4**, 3839-3844, doi:10.1039/C3SC51328A (2013).

3 Song, Z. Y. *et al.* Modulation of polypeptide conformation through donor-acceptor transformation of side-chain hydrogen bonding ligands. *Nat. Commun.* **8**, 92, doi:10.1038/s41467-017-00079-5 (2017).

4 Ikeda, T. Anionic Glycidyl Triazolyl Polymers: Oppositely Charged Analogs of Imidazolium-Based Cationic Glycidyl Triazolyl Polymers. *Macromolecules* **56**, 9229-9236, doi:10.1021/acs.macromol.3c01501 (2023).

5 Percec, V. *et al.* Modular Synthesis of Amphiphilic Janus Glycodendrimers and Their Self-Assembly into Glycodendrimersomes and Other Complex Architectures with Bioactivity to Biomedically Relevant Lectins. *J. Am. Chem. Soc.* **135**, 9055-9077, doi:10.1021/ja403323y (2013).

6 Shah, D. B. *et al.* Effect of Anion Size on Conductivity and Transference Number of Perfluoroether Electrolytes with Lithium Salts. *J. Electrochem. Soc.* **164**, A3511-A3517, doi:10.1149/2.0301714jes (2017).

7 Komar, A., Wilmer, D., Wilkening, H. M. R. & Hanzu, I. Accounting for stray capacitances in impedance measuring cells — A mandatory step in the investigation of solid ion conductors. *Solid State Ionics* **393**, 116169, doi:10.1016/j.ssi.2023.116169 (2023).

8 Song, Z. Y. *et al.* Synthesis of polypeptides via bioinspired polymerization of in situ purified N-carboxyanhydrides. *Proc. Natl. Acad. Sci. U. S. A.* **116**, 10658-10663, doi:10.1073/pnas.1901442116 (2019).

9 Xia, Y. C. *et al.* Accelerated polymerization of N-carboxyanhydrides catalyzed by crown ether. *Nat. Commun.* **12**, 732, doi:10.1038/s41467-020-20724-w (2021).

10 Fan, F. *et al.* Effect of Molecular Weight on the Ion Transport Mechanism in Polymerized Ionic Liquids. *Macromolecules* **49**, 4557-4570, doi:10.1021/acs.macromol.6b00714 (2016).

11 Zhao, Q. J. & Evans, C. M. Effect of Molecular Weight on Viscosity Scaling and Ion Transport in Linear Polymerized Ionic Liquids. *Macromolecules* **54**, 3395-3404, doi:10.1021/acs.macromol.0c02801 (2021).

12 Boyer, R. F. Variation of Polymer Glass Temperatures with Molecular-Weight. *Macromolecules* **7**, 142-143, doi:DOI 10.1021/ma60037a030 (1974).